HEALTH AND MEDICINE

Mitochondrial-targeted antioxidant attenuates preeclampsia-like phenotypes induced by syncytiotrophoblast-specific Gαq signaling

Megan A. Opichka[1], M. Christine Livergood[2], Kirthikaa Balapattabi[1], McKenzie L. Ritter[1], Daniel T. Brozoski[1], Kelsey K. Wackman[1], Ko-Ting Lu[1], Kaleigh N. Kozak[2], Clive Wells[3], Agnes B. Fogo[4], Katherine N. Gibson-Corley[4], Anne E. Kwitek[1,5,6], Curt D. Sigmund[1,5,7], Jennifer J. McIntosh[1,2,5]*, Justin L. Grobe[1,5,6,7,8]*

Syncytiotrophoblast stress is theorized to drive development of preeclampsia, but its molecular causes and consequences remain largely undefined. Multiple hormones implicated in preeclampsia signal via the Gαq cascade, leading to the hypothesis that excess Gαq signaling within the syncytiotrophoblast may contribute. First, we present data supporting increased Gαq signaling and antioxidant responses within villous and syncytiotrophoblast samples of human preeclamptic placenta. Second, Gαq was activated in mouse placenta using Cre-lox and DREADD methodologies. Syncytiotrophoblast-restricted Gαq activation caused hypertension, kidney damage, proteinuria, elevated circulating proinflammatory factors, decreased placental vascularization, diminished spiral artery diameter, and augmented responses to mitochondrial-derived superoxide. Administration of the mitochondrial-targeted antioxidant Mitoquinone attenuated maternal proteinuria, lowered circulating inflammatory and anti-angiogenic mediators, and maintained placental vascularization. These data demonstrate a causal relationship between syncytiotrophoblast stress and the development of preeclampsia and identify elevated Gαq signaling and mitochondrial reactive oxygen species as a cause of this stress.

INTRODUCTION

Hypertensive disorders of pregnancy, specifically preeclampsia, confer substantial maternal-fetal health risks during gestation and in the postpartum period (*1*–*5*). Preeclampsia is diagnosed based on the presence of new-onset hypertension and end organ dysfunction after 20 weeks of gestation (*6*). Current incidence rates are rising (*7*, *8*), yet detailed mechanistic insight and effective treatment options are limited. Despite these shortcomings, it is well-established that the placenta has a prominent role in its pathogenesis (*9*, *10*), and experts have theorized that generalized syncytiotrophoblast stress may be a final common factor in the development of this syndrome regardless of the initiating factor (*11*).

As the forefront of the maternal-fetal interface, syncytiotrophoblast cells comprise the outer villous layer of the placenta and are essential for material exchange and hormone production (*12*). Throughout pregnancy, this layer is susceptible to damage (*13*) and can release stress-induced bioactive factors, extracellular vesicles, and cell-free DNA into the maternal circulation (*14*, *15*). Preeclampsia is accompanied by exacerbated oxidative, mitochondrial, and endoplasmic reticulum stress, ultimately contributing to enhanced propagation of these signals (*16*–*19*). Although a wide array of correlative evidence recapitulates the involvement of syncytiotrophoblast stress in the clinical presentation of preeclampsia (*16*–*19*), the causality of this relationship and the precise origins have yet to be established.

Many animal studies use hypoxia-related insults such as placental ischemia (*20*–*22*) or anti-angiogenic factors (*23*, *24*) to model preeclampsia. However, there is increasing appreciation that hypoxia is just one of many molecular signatures of the disorder (*25*–*27*), and Gαq-coupled pressure-related hormones, particularly vasopressin, angiotensin II, and endothelin-1, are also independently implicated (*28*–*30*). Rodent and ex vivo human experiments reveal that augmented signaling via these circulating substances causes systemic hallmarks of preeclampsia, alters placental morphology, and impairs oxidative buffering (*26*, *31*, *32*). Further, placental expression of regulator of G protein signaling-2 (*RGS2*), a major terminator of Gαq activation (*33*, *34*), is decreased during preeclampsia (*35*). Reduced placental expression of *Rgs2* in the fetoplacental unit of mice is sufficient to induce clinical features of preeclampsia and placental transcriptomic profiles reflective of mitochondrial dysfunction, an unfolded protein response, and oxidative stress (*35*). Excess production of mitochondrial-derived reactive oxygen species within trophoblast cell cultures disrupts mitochondrial dynamics, perturbs hormone production, and reduces trophoblast fusion, which is critical for syncytiotrophoblast formation (*36*).

We hypothesized that elevated Gαq stimulation within the syncytiotrophoblast layer contributes to the pathogenesis of preeclampsia through disruption of normal redox balance and thus the induction of syncytiotrophoblast stress. Our studies provide evidence of increased Gαq signaling within syncytiotrophoblasts of human placenta during preeclampsia, the sufficiency of selective

[1]Department of Physiology, Medical College of Wisconsin, Milwaukee, USA. [2]Department of Obstetrics and Gynecology, Medical College of Wisconsin, Milwaukee, USA. [3]Electron Microscopy Core Facility, Medical College of Wisconsin, Milwaukee, USA. [4]Department of Pathology, Microbiology and Immunology, Vanderbilt University Medical Center, Nashville, USA. [5]Cardiovascular Center, Medical College of Wisconsin, Milwaukee, USA. [6]Department of Biomedical Engineering, Medical College of Wisconsin, Milwaukee, USA. [7]Neuroscience Research Center, Medical College of Wisconsin, Milwaukee, USA. [8]Comprehensive Rodent Metabolic Phenotyping Core, Medical College of Wisconsin, Milwaukee, USA.
*Corresponding author. Email: jgrobe@mcw.edu (J.L.G.); jmcintosh@mcw.edu (J.J.M.)

induction of Gαq signaling within syncytiotrophoblasts of mouse placenta to cause preeclampsia-like phenotypes, and a critical role for mitochondrial redox functions in this process. These studies provide unique critical mechanistic evidence supporting the "syncytiotrophoblast stress" theory of preeclampsia and provide insight toward targetable pathways and available pharmacological agents that may be used to slow progression of this gestational disorder.

RESULTS

Increased Gαq-related activity is observed in human placenta during preeclampsia

Phospholipase C (PLC) is a critical enzyme mediating actions of the Gαq second messenger system (Fig. 1A) (*37*). Therefore, its activity was assessed as a metric of Gαq signaling. PLC activity was augmented in third-trimester villous placenta samples derived from human pregnancies complicated by preeclampsia compared to control pregnancies ($P = 0.009$; Fig. 1C).

Reanalysis of a large human placental microarray dataset (GSE75010) corroborates these findings as in term preeclampsia there was an enrichment in up-regulated genes related to the PLC-activating G protein–coupled receptor signaling pathway

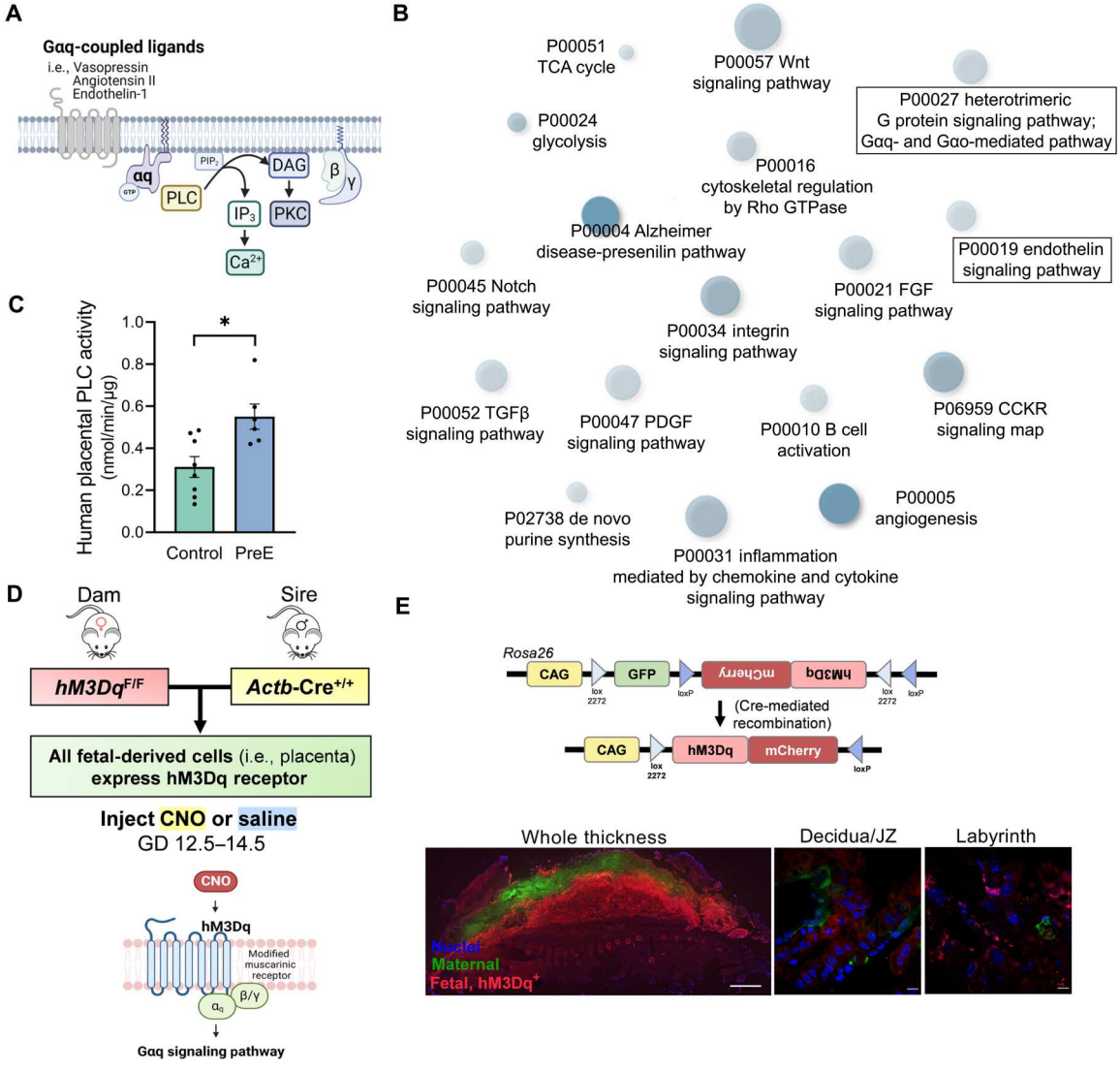

Fig. 1. Augmented Gαq-related activity in human preeclamptic placenta and development of a mouse model of fetoplacental Gαq signaling. (**A**) Overview of Gαq-mediated signaling pathway. (**B**) Gene ontology biological processes (Shiny GO 0.74.1) enriched within the differentially expressed gene set of preterm preeclamptic placenta compared to preterm control (microarray, GSE75010; preterm control $n = 35$, preterm PreE $n = 49$). (**C**) PLC activity in human villous placental samples. (**D**) Breeding paradigm for targeting hM3Dq expression to the placenta and schematic depicting selective activation of the Gαq cascade with the hM3Dq DREADD. (**E**) Schematic of *Cag*-FLEX-*hM3Dq* in the *Rosa26* locus (top), adapted from (*40*). Placenta of *hM3Dq* dam x *Actb*-Cre sire pregnancy. Scale bars, 1000 μm (left) and 10 μm (middle, right). PreE, preeclampsia. TCA, tricarboxylic acid. GTPase, guanosine triphosphatase. JZ, junctional zone. Images (A, D, and E) were created using BioRender (www.biorender.com).

compared to term control (Table 1). Similarly, preterm preeclampsia was also marked by differential expression of canonical genes involved in the heterotrimeric Gαq protein signaling pathway and its downstream events (Fig. 1B), including those provoked by endothelin-1 (Fig. 1B and fig. S1), the angiotensin II type 1 receptor (fig. S1), and chemokine–chemokine receptor interactions (fig. S2). Further, as mitochondrial inefficiencies can be both a cause and consequence of oxidative stress (*38*), preterm preeclamptic placentas also exhibited gene expression patterns indicative of down-regulated mitochondrial respiratory chain complex I assembly, adenosine 5′-triphosphate (ATP) synthesis coupled electron transport, and generation of precursor metabolites and energy (fig. S3).

Gαq activation throughout the fetoplacental unit of mice induces preeclampsia-like phenotypes

To explore the consequences of excess Gαq signaling within the fetoplacental unit of mice upon maternal-fetal outcomes, we used a Cre-lox genetic strategy to cause expression of the Gαq-coupled hM3Dq Designer Receptor Exclusively Activated by Designer Drug (DREADD) in a tissue-specific manner. The hM3Dq DREADD enables the selective activation of the Gαq pathway in response to a synthetic exogenous ligand, clozapine *N*-oxide (CNO) (Fig. 1D) (*39*). To target hM3Dq expression only to the fetoplacental unit, dams harboring a Cre-activable hM3Dq construct were bred with sires expressing Cre via the ubiquitous *Actb* promoter (Fig. 1D). The hM3Dq construct is located within the *Rosa26*

Table 1. Comparison of placental transcriptomic signatures (Shiny GO Biological Processes 0.76.1) following syncytiotrophoblast-restricted Gαq stimulation in mice (bulk RNA sequencing; *n* = 6 per group, GD 14.5) to those implicated in human preeclampsia (PreE) (microarray, GSE75010; term control *n* = 28, term PreE *n* = 31). Symbol "—" indicates that enrichment did not meet threshold of false discovery rate (FDR) < 0.15. Superscripts 1 and 2 refer to similar gene ontology (GO) terms that had slightly different representation among groups.

Up-regulated GO biological processes	Fold enrichment (CNO Cre$^+$ versus saline)	FDR	Fold enrichment (CNO Cre$^+$ versus CNO Cre$^-$)	FDR	Fold enrichment (human PreE versus control)	FDR
Gαq related						
PLC-activating angiotensin-activated signaling pathway[1]	41.7[1]	0.01[1]	—	—	2.2[2]	0.05[2]
PLC-activating G protein–coupled receptor signaling pathway[2]						
G protein–coupled receptor signaling pathway involved in heart process	34.1	0.003	—	—	—	—
Angiotensin-activated signaling pathway	17.9	0.04	—	—	—	—
Positive regulation of calcium ion import[1]	14.4[1]	0.02[1]	4.7[2]	0.06[2]	1.9[2]	0.03[2]
Calcium-mediated signaling[2]						
Second messenger–mediated signaling	4.8	0.0005	4.6	0.01	1.6	0.07
Oxidative stress						
Positive regulation of reactive oxygen species metabolic process	8.9	0.007	—	—	2.8	0.02
Superoxide metabolic process	5.8	0.09	—	—	—	—
Cellular response to oxidative stress	3.2	0.05	3.2	0.13	1.6	0.09
Hypoxia						
Response to hypoxia	4.6	0.0007	—	—	1.9	0.002
Vascular						
Smooth muscle contraction	7.9	0.002	—	—	2.4	0.02
Negative regulation of angiogenesis	6.9	0.007	4.9	0.14	2.3	0.03
Immune						
Positive regulation of CD4$^+$, α-β T cell proliferation	83.4	0.006	—	—	—	—
Leukocyte adhesion to vascular endothelial cell	8.7	0.04	8.3	0.15	2.6	0.09
Positive regulation of inflammatory response	6.0	0.01	—	—	1.9	0.06
Positive regulation of leukocyte cell-cell adhesion	4.7	0.008	4.2	0.08	1.7	0.05
Positive regulation of T cell activation	4.5	0.02	—	—	1.7	0.05

locus and consists of a strong ubiquitous *Cag* promoter that drives green fluorescent protein (GFP) until Cre-mediated recombination. After recombination, GFP is lost, and hM3Dq fused with the red florescent mCherry reporter is expressed (Fig. 1E) (*40*). Fluorescent imaging was used for model verification, and as expected, maternal (i.e., Cre-deficient) cells express GFP whereas cells of fetal origin (i.e., placenta) express mCherry (Fig. 1E).

Pregnant females carrying double-transgenic ($hM3Dq^+$, Cre^+) fetoplacental units received daily injections of CNO (2 mg/kg per day, i.p.) or saline (2 ml/kg per day, i.p.) mid-gestation [gestational day (GD) 12.5 to 14.5] before maternal and fetoplacental assessments following the third injection at GD 14.5. This injection period coincides with the time of mature chorioallantoic placental formation (*41*) and developmentally aligns with the second trimester in humans (*42*). This low dose of CNO was chosen to avoid back-metabolism to the pharmacologically active molecule, clozapine, (*43*) and had no discernible effects independent of the hM3Dq receptor in our explored endpoints (fig. S1 and table S1).

Activation of hM3Dq by CNO induced multiple preeclampsia-like phenotypes including proteinuria ($P = 0.026$; Fig. 2A), increased maternal circulating soluble *fms*(Feline McDonough Sarcoma)-like tyrosine kinase 1 (sFLT1) ($P = 0.032$; Fig. 2B), and reduced placental vascular endothelial growth factor (VEGF) protein ($P = 0.010$; Fig. 2C). These data suggest an angiogenic imbalance, as sFLT1 is a truncated form of the VEGF receptor 1 that binds to pro-angiogenic VEGFA and placental growth factor (PlGF) to render them inactive (*44*, *45*). Histopatholgic findings in the kidney were absent as assessed by light microcopy within hematoxylin and eosin–stained tissue (Fig. 2D). Total vascularization within each region of the mouse placenta was evaluated by immunostaining for platelet endothelial cell adhesion molecule (CD31). The area of CD31-positive placenta within the labyrinth, responsible for exchange, was severely attenuated ($P = 0.0038$; Fig. 2, E and F). In contrast, vascular patterning was retained within the decidua ($P = 0.52$) and junctional zone ($P = 0.97$), a major director of endocrine function (*46*). Placental histological lesions were indicative of maternal vascular dysfunction and inflammation, evidenced by the presence of decidual vascular congestion, nuclear debris, fibrin deposition, neutrophil infiltration, and necrosis in hematoxylin and eosin–stained tissue (Fig. 2G and fig. S4). Overall, this stimulus represented a massive insult to pregnancy, resulting in frequent spontaneous abortion (3 of 7 pregnancies) and nonviable fetuses (26 of 26). These data confirm that amplified Gαq signaling within the fetoplacental unit has a profound effect on multiple pregnancy outcomes; however, the severity of the phenotypes induced in this model and the lack of cellular specificity prompted additional studies of the prevalence and effects of Gαq activation in individual layers of placenta, focusing upon the syncytiotrophoblast layer.

Elevated Gαq signaling and oxidative stress are present in human syncytiotrophoblasts during preeclampsia

To evaluate the status of the Gαq cascade and oxidative stress specifically within the syncytiotrophoblast layer of human placenta, we next performed laser capture microdissection to collect syncytiotrophoblast-enriched cellular fractions (Fig. 3, A and B). The protein expression of PLCβ1/3, signature Gαq effectors (*37*), was elevated in preeclamptic syncytiotrophoblasts compared to controls ($P = 0.035$; Fig. 3C). Although PLC is an enzyme and thus more reliably assessed at an activity level, the dehydration procedures required for laser capture microdissection and the small quantity of collected tissue render these samples incompatible for this activity assay. However, syncytiotrophoblasts comprise a large percentage of the villous tree, and correlation analysis revealed a positive association between villous PLC activity and syncytiotrophoblast PLCβ protein content (Pearson $R = 0.74$, $P = 0.014$; Fig. 3D). During Gαq signal transduction, PLC cleaves phosphoinositide 4,5-bisphosphate to inositol 1,4,5-trisphosphate (IP_3) (*47*). IP_3 binding to its receptors within the endoplasmic reticulum leads to the liberation of calcium (*47*), which controls a broad array of cellular events [i.e., activation of kinases and transcription factors (*48*) and vesicular release (*49*)]. IP_3 receptor (ITPR3) mRNA was also increased in preeclamptic syncytiotrophoblasts ($P = 0.04$; Fig. 3E).

Superoxide dismutase-2 (SOD2) is a protective mitochondrial matrix enzyme that catalyzes the conversion of superoxide to hydrogen peroxide (*50*), and excess free radicals lead to the generation of malondialdehyde (MDA), a final product of lipid peroxidation (Fig. 3F) (*51*). SOD2 mRNA ($P = 0.027$) and protein ($P = 0.047$; Fig. 3G) as well as MDA protein ($P = 0.03$; Fig. 3H) were increased within preeclamptic syncytiotrophoblasts (Fig. 3F), and there appears to be a positive correlation between the protein expression of PLCβ and SOD2 within these cells (Pearson $R = 0.70$, $P = 0.012$; fig. S5). Collectively, these data support the concept that syncytiotrophoblast Gαq signaling facilitates an oxidant defense response within this placental layer and may be involved in the pathophysiology of preeclampsia.

Syncytiotrophoblast-restricted Gαq stimulation in mice results in impaired placental development driven by mitochondrial-derived reactive oxygen species

The syncytiotrophoblast-specific *Gcm1*-Cre driver (*52*) was used to drive expression of the hM3Dq DREADD only within this layer of mouse placenta (Fig. 4, A and B). Homozygous hM3Dq dams were bred with hemizygous sires expressing Cre via the *Gcm1* promoter to elicit syncytiotrophoblast II–restricted (*52*) expression of hM3Dq in ~50% of fetoplacental units. This breeding paradigm allowed paired comparisons between Cre^+ and Cre^- placentas within a dam while also avoiding any unintended epigenetic effects of passing the imprinted *Gcm1*-Cre transgene through the maternal germ line. Thus, the direct effects of Gαq activation within the syncytiotrophoblast layer upon the structure and function of that placenta can be evaluated (i.e., CNO-treated Cre^+ placenta versus saline-treated). Simultaneously, endocrine effects evoked by circulating factors can be explored by examining phenotypes of Cre^- placentas collected from CNO-treated dams that also carried Cre^+ placentas. As used in the fetoplacental model (Fig. 1), the DREADD ligand CNO (2 mg/kg per day, i.p.) or saline (2 ml/kg per day, i.p.) was injected daily during GD 12.5 to 14.5, before fetoplacental analyses at GD 14.5.

Because of the design of the hM3Dq vector, the hM3Dq-mCherry fusion protein should be present in *Gcm1*-positive syncytiotrophoblast II cells and GFP in all other cells. Florescent imaging validated hM3Dq targeting to the proper placental region, indicated by mCherry expression only within a subset of labyrinth cells, along with broad GFP expression within the decidual and junctional zones (Fig. 4C). Similarly, in situ hybridization confirmed colocalization of *Cre* and *Gcm1* transcripts within the labyrinth (Fig. 4D).

To test our secondary hypothesis that the detrimental effects of exacerbated Gαq signaling depend on excess mitochondrial

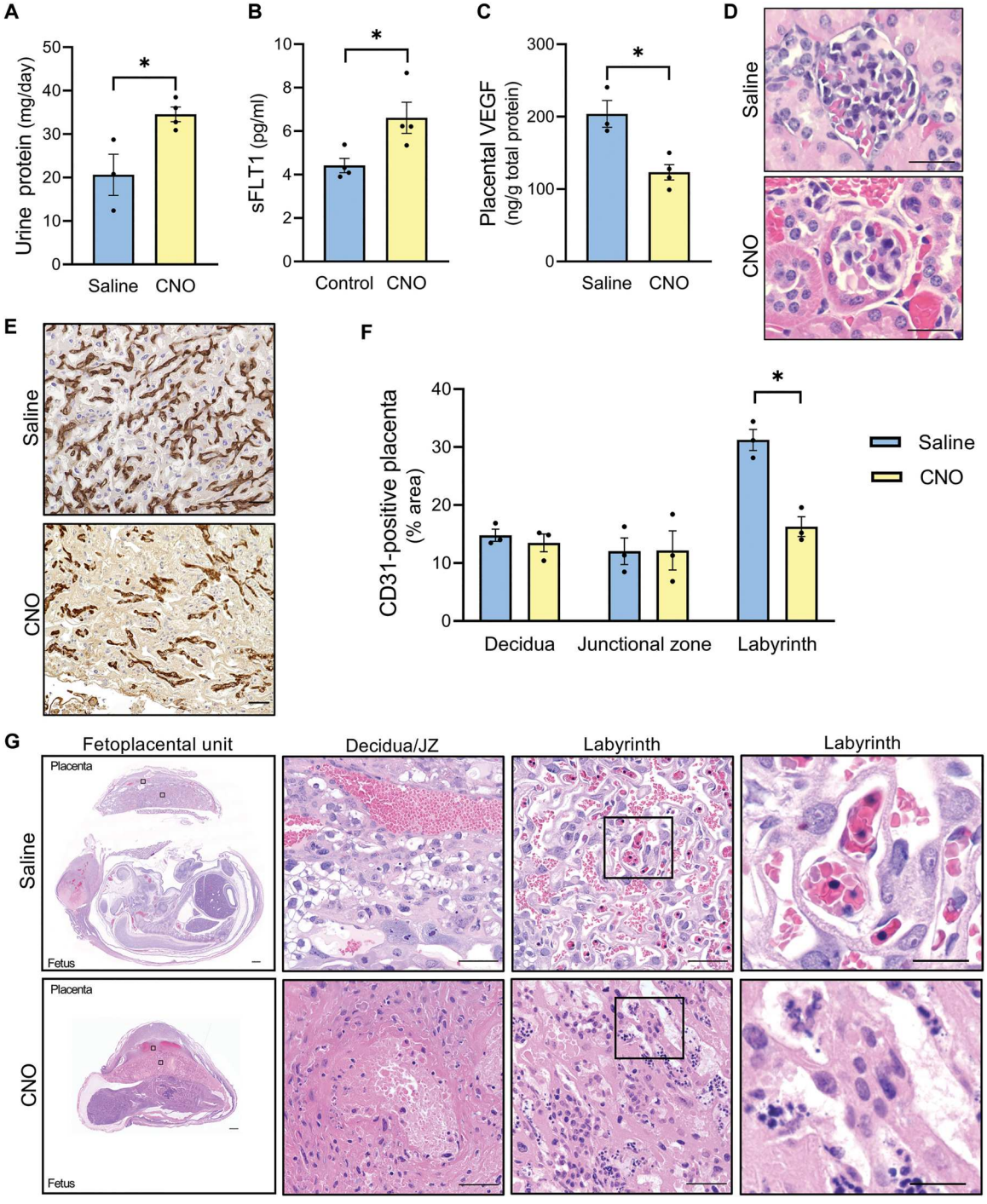

Fig. 2. Exogenous fetoplacental Gαq activation leads to severe pregnancy impairments in mice (*hM3Dq*$^{F/F}$ dam x *Actb*-Cre$^{+/+}$ sire, GD 14.5). (**A**) Twenty-four–hour maternal urine protein excretion. (**B**) Maternal plasma sFLT1. (**C**) Placental VEGF protein levels. (**D**) Hematoxylin and eosin stain of glomeruli. Scale bars, 25 μm. (**E**) Representative labyrinth image of diaminobenzidine (DAB) immunostained for CD31. Scale bars, 50 μm. (**F**) Percentage area of CD31-positive placenta. (**G**) Hematoxylin and eosin stain of fetoplacental unit. Scale bars, 500 μm (left), 50 μm (middle), and 10 μm (right). Each datapoint represents a biological replicate. *$P < 0.05$, independent samples *t* test (two-tailed).

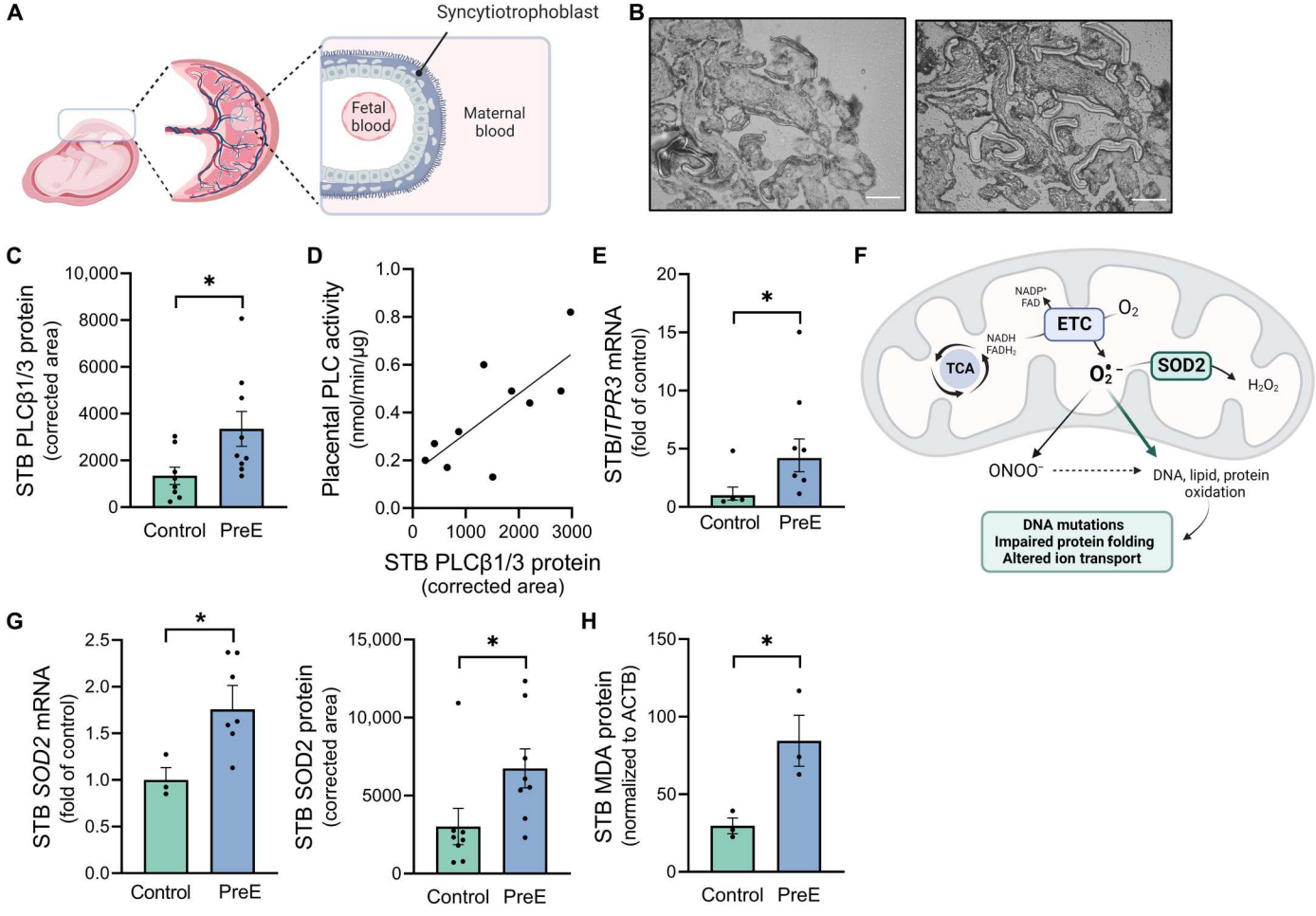

Fig. 3. Evidence of increased Gαq signaling and an oxidative defense response in human syncytiotrophoblast cells during preeclampsia. (**A**) Diagram of syncytiotrophoblast layer within human placenta. (**B**) Laser capture microdissection was performed to collect syncytiotrophoblast-enriched cellular fractions. Scale bars, 100 μm. (**C**) PLCβ1/PLCβ3 protein expression within syncytiotrophoblast. (**D**) Correlation between villous placental PLC activity and syncytiotrophoblast PLCβ1/PLCβ3 protein levels. (**E**) *ITPR3* mRNA within syncytiotrophoblast. (**F**) Overview of superoxide buffering by SOD2 in the mitochondrial matrix and the cellular effects of excess superoxide, adapted from (*75*). (**G**) *SOD2* mRNA and protein expression within syncytiotrophoblast. (**H**) MDA protein expression within syncytiotrophoblast; *$P < 0.05$, independent samples *t* test (two-tailed) (C, G, and H) and Mann-Whitney *U* test (E). Each datapoint represents a biological replicate. STB, syncytiotrophoblast. Images (A and F) were created using BioRender (www.biorender.com).

production of reactive oxygen species, the mitochondrial-targeted antioxidant Mitoquinone (MitoQ) was coadministered (5 mg/kg per day, i.p.) with CNO in a cohort of double-transgenic (hM3Dq$^+$, Gcm1-Cre$^+$) pregnancies. Control experiments revealed that MitoQ had no observed effects within the context of normal pregnancy (figs. S6 and S7 and table S1), consistent with minimal negative effects of reactive oxygen species when present at controlled concentrations (*53*).

Stimulation of Gαq by CNO within hM3Dq$^+$, Gcm1-Cre$^+$ cells was supported by changes in the placental transcriptomic landscape indicative of up-regulated PLC-activating angiotensin-activated signaling, second messenger– and calcium-mediated signaling, and expression patterns reflective of neuroactive ligand interactions with receptors known to couple to Gαq (Table 1 and fig. S8). Structurally, this syncytiotrophoblast-specific model primarily exhibited placental vascular defects. Decidual spiral artery diameter was attenuated following syncytiotrophoblast-localized Gαq induction (CNO Cre$^+$) compared to saline ($P = 0.038$; Fig. 5A and fig. S7). Furthermore, the fraction of CD31-positive labyrinth, the region containing syncytiotrophoblasts (*46*), was reduced within CNO-injected double-transgenic placentas versus controls, including both paired Cre$^-$ placentas within the same dam ($P = 0.0013$) and placentas obtained from dams that received saline vehicle injections instead of CNO ($P = 0.016$; Fig. 5, B and C). In contrast, CD31-positive area within the decidua and junctional zone remained unaffected by Gαq activation. Decidual thickness was also decreased in paired CNO Cre$^+$ versus CNO Cre$^-$ placentas ($P = 0.0024$; Fig. 5D). The ratio between fetal mass and placental mass (F/P) is often used as a proxy for placental efficiency, indicative of nutrient transfer per gram of placenta (*54*). Within CNO-injected double-transgenic dams, there was a decline in placental mass ($P = 0.0034$) and fetal mass ($P = 0.0032$) as well as F/P ratio ($P = 0.016$) in Cre$^+$ fetoplacental units (Fig. 5E). Of the affected parameters, MitoQ treatment mitigated Gαq-related impairments in labyrinth vascularization ($P = 0.038$; Fig. 5, B and C) and spiral artery diameter ($P = 0.0055$; Fig. 5A and fig. S7), although larger

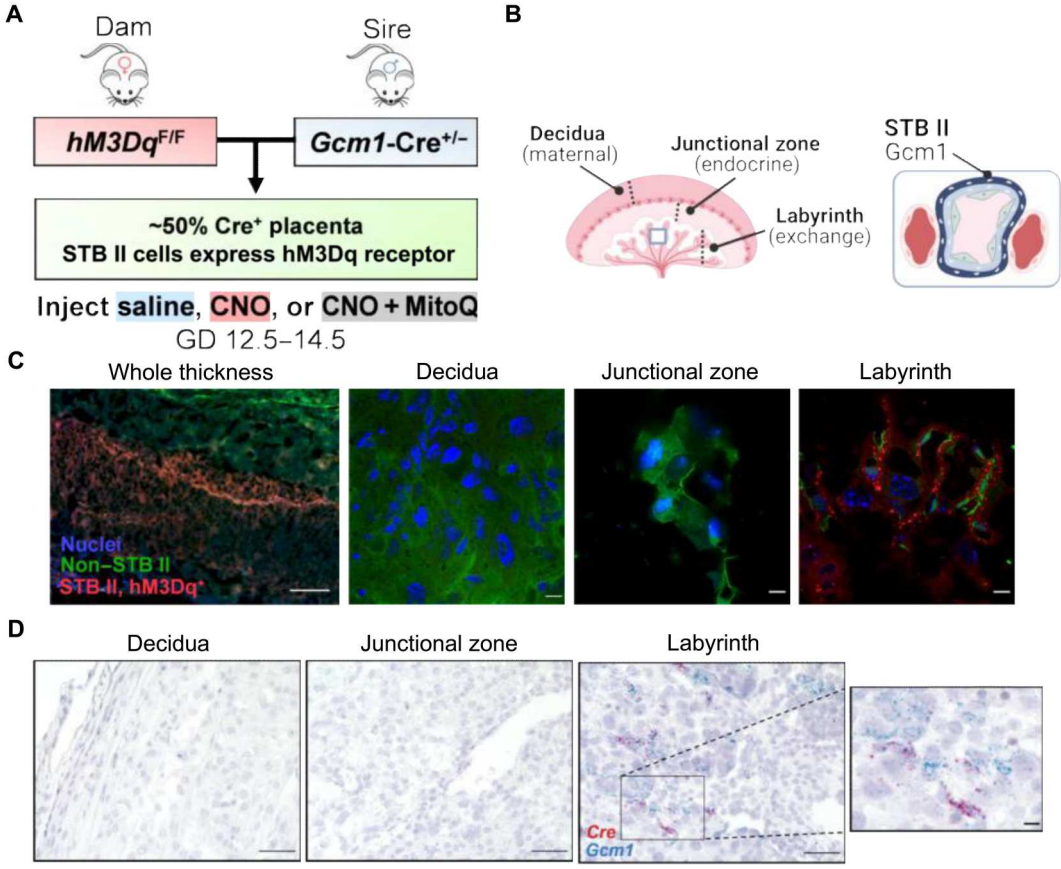

Fig. 4. Mouse model of syncytiotrophoblast-specific Gαq stimulation with mitochondrial-targeted antioxidant administration. (**A**) Breeding paradigm for selective activation of the Gαq pathway in only the syncytiotrophoblast II layer. (**B**) General anatomy of the mouse placenta. (**C**) Double-transgenic placenta of *hM3Dq*$^{F/F}$ dam x *Gcm1*-Cre$^{+/-}$ sire. Scale bars, 300 μm (left) and 10 μm (middle, right). (**D**) RNAscope-based in situ hybridization of double-transgenic placenta. Scale bars, 50 μm and 10 μm (inset on right). STB II, syncytiotrophoblast II layer. Images (A and B) were created using BioRender (www.biorender.com).

morphological changes were not manifested after only 2 days of treatment (Fig. 5, D and E). Collectively, these data demonstrate that enhanced Gαq propagation within syncytiotrophoblasts causes maladaptive changes in vascular supply to the placenta, and this effect is dependent on oxidative stress.

Hypoxia-inducible factor 1 (HIF1) is a canonical transcription factor that contributes to cellular responses to low oxygen tension (*55*), and its HIF1α subunit is activated (i.e., translocated into the nucleus) in the presence of hypoxia (*56*). Consistent with the induction of a hypoxia response, nucleus-localized HIF1α protein was increased within CNO-treated Cre$^+$ placentas ($P = 0.044$ versus paired Cre$^-$, $P = 0.032$ versus saline; Fig. 5F). In addition, bulk RNA sequencing revealed an enrichment of genes related to hypoxic response pathways in CNO-treated Cre$^+$ placentas compared to saline controls (Table 1). At an individual gene level, transcripts for several previously identified HIF1α targets were elevated in CNO-treated Cre$^+$ placentas versus paired Cre$^-$ or saline samples (table S2). In contrast, the protein content of VEGFA, a well-recognized HIF1 target (*57*, *58*), and its homolog, PlGF (*59*), were unchanged in labyrinth-enriched placentas (fig. S9). Together, these results support the conclusion that induction of Gαq in the syncytiotrophoblast layer is adequate to initiate selected transcriptional signatures of a hypoxic response within the placenta; nonetheless, this relatively brief and cell-restricted stimulation is insufficient to cause robust changes in typical angiogenic proteins.

Consistent with our human placental data (Fig. 3), activation of the Gαq pathway within the syncytiotrophoblast layer in mice elicited an oxidative defense response, demonstrated by elevated labyrinth SOD2 protein expression compared to saline controls ($P = 0.0003$; Fig. 5G). Despite this rise, catalase protein levels were not significantly altered (Fig. 5H), and the lipid peroxidation marker MDA was increased ($P = 0.003$ versus saline, $P = 0.03$ versus CNO Cre$^-$; Fig. 5I, indicating an inability to adequately buffer the reactive oxygen species present, particularly superoxide and hydrogen peroxide. Simultaneous administration of MitoQ prevented the rise in SOD2 ($P = 0.0006$) and MDA ($P = 0.0535$), suggesting that the increased free radical buffering capacity provided by this compound was protective against Gαq-perpetuated oxidative damage. Changes in mitochondrial morphology were also evaluated by electron microscopy (Fig. 5J), which indicated the greatest degree of damage in CNO Cre$^+$ placentas compared to those that received saline or CNO + MitoQ. Within CNO Cre$^+$ samples, the placental mitochondria generally appeared smaller and more circular, with the exception of some that were large and swollen with dilated cisternae and amorphous precipitate. MitoQ did not completely abolish mitochondrial injury as they exhibited some occasional

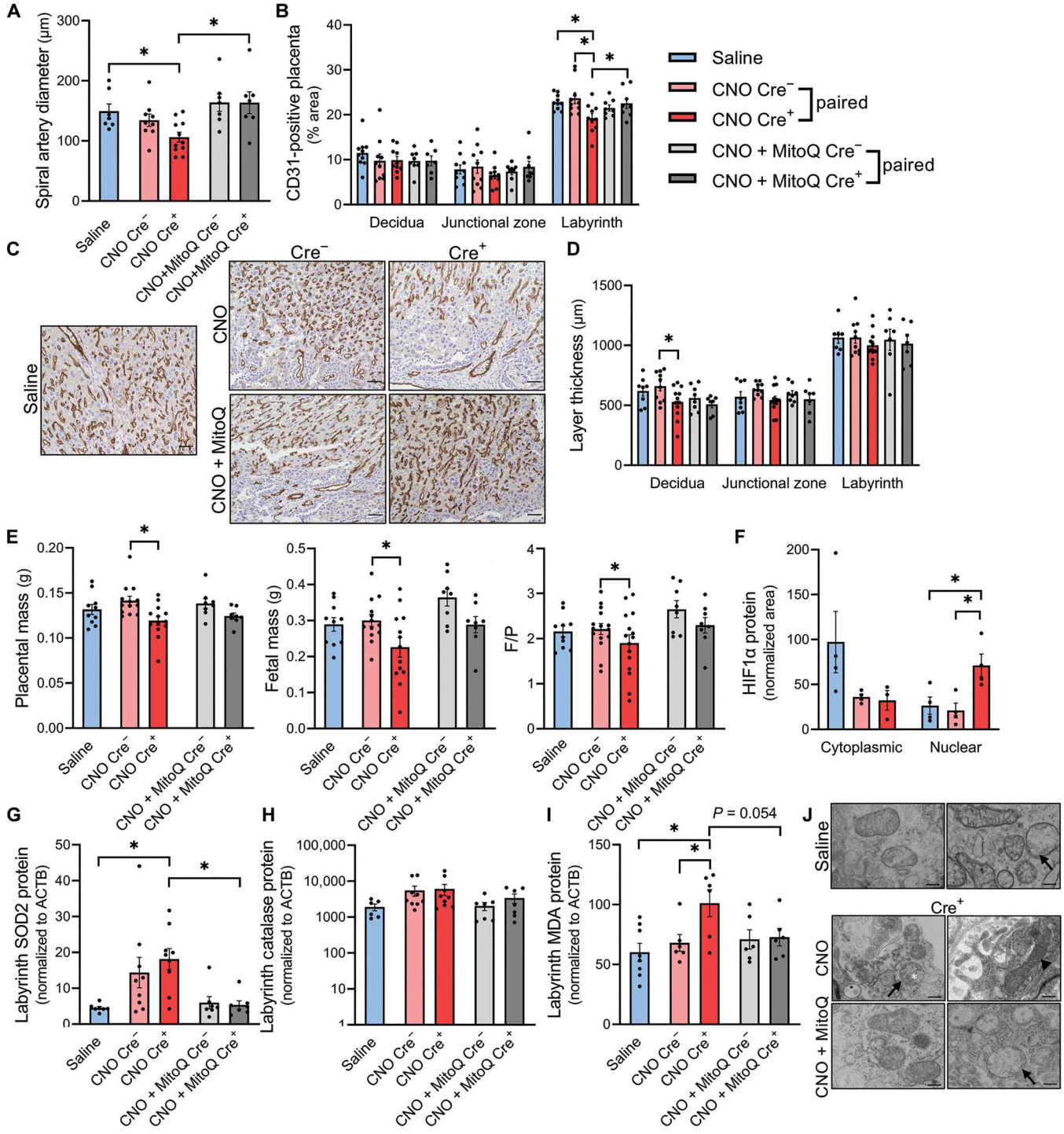

Fig. 5. Placental effects of syncytiotrophoblast-localized Gαq (*hM3Dq*$^{F/F}$ dam x *Gcm1*-Cre$^{+/-}$ sire, GD 14.5). (**A**) Average luminal diameter of decidual spiral arteries. (**B**) Percentage area of CD31-positive placenta. (**C**) Representative labyrinth image of DAB immunostain for CD31. Scale bars, 50 µm. (**D**) Thickness of each placental layer. (**E**) Placental mass, fetal mass, and fetal mass/placental mass. (**F**) Soluble cytoplasmic (normalized to ACTB) and nuclear HIF1α (normalized to HDAC1) protein abundance. (**G** to **I**) SOD2, catalase, and MDA protein expression in labyrinth-enriched dissections. (**J**) Transmission electron micrographs of placental mitochondria. Arrows indicate occasional swelling. White asterisk denotes amorphous electron-dense precipitate, and arrowhead highlights a condensed mitochondrion. Scale bars, 300 nm; *$P < 0.05$, one-way analysis of variance (ANOVA) with Bonferroni multiple comparisons procedure, independent samples *t* test (two-tailed), or paired samples *t* test (two-tailed). Each datapoint represents a biological replicate.

swelling. However, several mitochondria within this cohort resembled those of the healthy saline group, and there was also qualitatively more total volume of mitochondria.

Many of these structural and molecular findings are corroborated by RNA sequencing and align with those prevalent in human preeclampsia (Table 1). Within the up-regulated and differentially expressed gene set, there was an enrichment in superoxide metabolic process, positive regulation of reactive oxygen species, smooth muscle contraction, regulations of cell migration and epithelium development, wound healing, negative regulation of angiogenesis, and other inflammatory signatures within CNO Cre^{+} placentas relative to saline and CNO Cre^{-} controls (Table 1 and figs. S10 to S13). More specifically, the altered transcripts and regulatory networks indicate that these signatures and phenotypes can be attributed to enhanced major histocompatibility complex class I (MHC I) and MHC II antigen presentation to CD4^{+} and CD8^{+} T cells (fig. S14) as well as control of cyclin D–dependent cell cycle arrest, tumor necrosis factor–related apoptosis-inducing ligand (TRAIL), and krüppel-like factor 2–mediated immune-regulation via transforming growth factor–β (TGFβ) receptor, macrophage stimulating protein, serum glucocorticoid regulated kinase, and forkhead box G1 (FoxG1) (figs. S14 and S15). Further, syncytiotrophoblast-localized Gαq stimulation also led to diminished mRNA encoding the enzymes glutamic-pyruvic transaminase 2, quinolinate phosphoribosyltransferase, methylenetetrahydrofolate dehydrogenase, phosphoserine aminotransferase 1,3-hydroxyanthranilate dioxygenase,

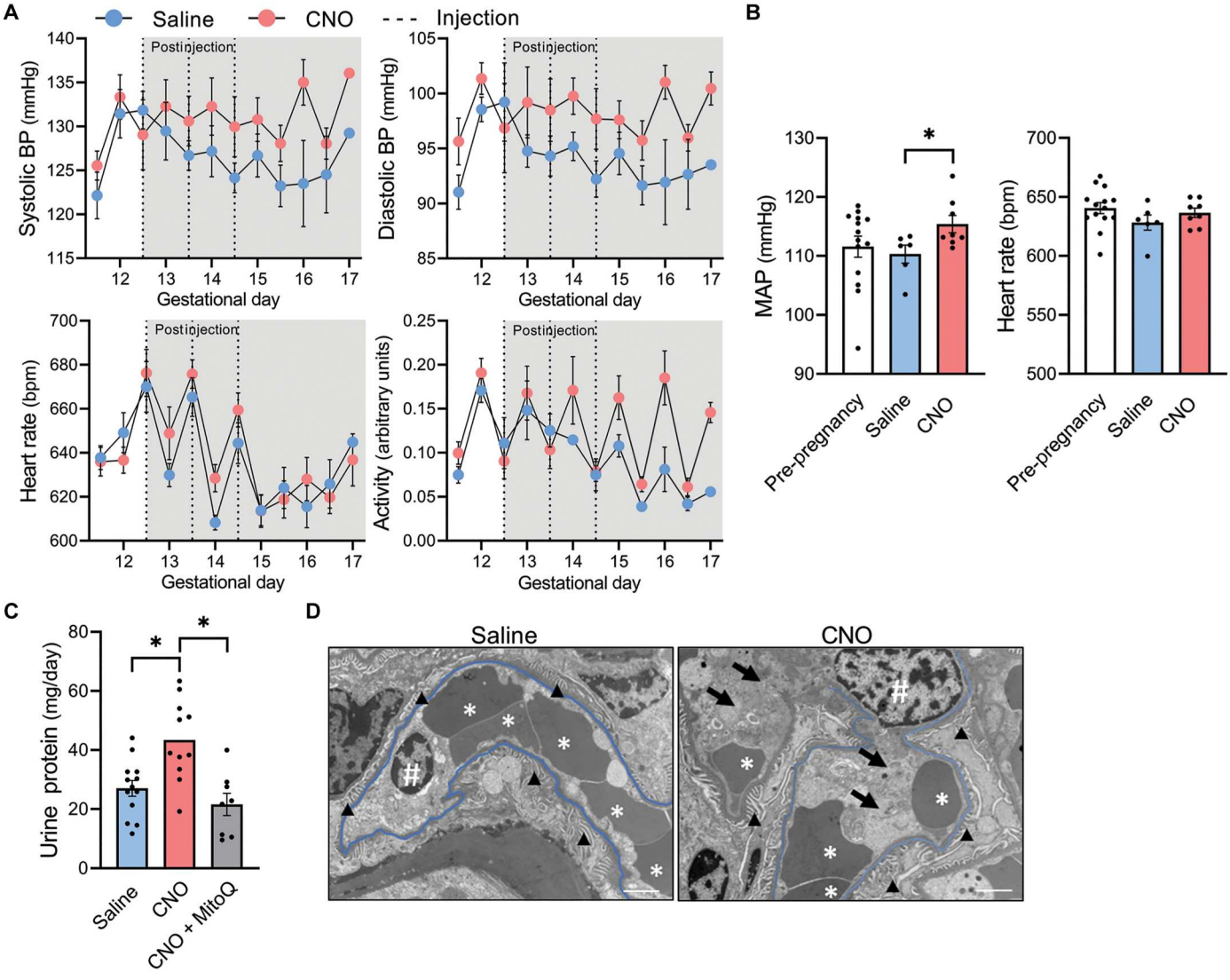

Fig. 6. Maternal effects of syncytiotrophoblast-restricted Gαq activation (*hM3Dq*$^{F/F}$ dam x *Gcm1*-Cre$^{+/-}$ sire). (**A**) Average daily systolic blood pressure, diastolic blood pressure, heart rate, and activity separated by light and dark cycles. Dotted lines indicate time of CNO or saline administration (to GD 16.5: saline $n = 6$, CNO $n = 8$; to GD 17: saline $n = 1$, CNO $n = 4$). (**B**) Average 24-hour heart rate and mean arterial pressure (MAP) from GD 13 to 16.5 (postinjection period). (**C**) Twenty-four–hour urine protein excretion at GD 14.5. (**D**) Transmission electron micrographs of renal capillary loops at GD 14.5 indicating slight endothelial swelling in CNO mice (arrows) and slight congestion in both groups (* denotes red blood cells). Capillary basement membranes are highlighted in blue. Symbol "#" represents endothelial cell nuclei. Arrowheads identify podocyte foot processes. Scale bars, 2 μm; *$P < 0.05$, independent samples *t* test (two-tailed) or one-way ANOVA with Bonferroni multiple comparisons procedure. Datapoints for (B) and (C) represent biological replicates. BP, blood pressure.

and serine dehydratase-like protein, which are known to play a role in the biosynthesis of nicotinamide adenine dinucleotide, purines, thymidylate, pyruvate, and amino acids (figs. S16 and S17). This down-regulation may have ultimately contributed to impaired metabolism, nucleotide synthesis, nutrient transport, and overall placental function.

Within CNO-treated Cre$^+$ placentas, coadministration of MitoQ led to transcriptomic profiles related to negative regulation of G protein–coupled receptor (GPCR) signaling and apoptotic processes, responses to reactive oxygen species, positive regulation of vasculature development, and epithelial cell differentiation (Table 2). Of the highlighted mediators, FoxG1, cyclin D, and TRAIL were decreased compared to CNO alone (fig. S18). Other altered controllers of differentiation, immunity, tissue remodeling, apoptosis, and lipid accumulation included interleukin-1, TGFβ, activator protein 1, c-Fos, matrix metalloproteinase 13, interferon regulatory factor 7, mitochondrial B cell lymphoma-extra large, organic cation transporter 1, Fas, and ATP binding cassette transporter G1 (figs. S19 to S21). MitoQ also enhanced transcription of several proteins necessary for protein processing in the endoplasmic reticulum (fig. S22) and decreased tumor suppressor-activated pathway 6 (*Tsap6*/*Steap3*) involved in exosome-mediated secretion (fig. S23), suggesting attenuated placental release of biological factors that may disrupt maternal physiology and fetal development.

Collectively, these placental characterizations demonstrate that enhanced Gαq signaling within the syncytiotrophoblast layer alone facilitates morphological and molecular changes that parallel features of human preeclampsia, many of which are driven by mitochondrial-derived reactive oxygen species.

Table 2. Enriched pathways in up-regulated gene set (Shiny GO Biological Processes 0.76.1) of CNO + MitoQ Cre$^+$ placentas compared to CNO Cre$^+$ determined by bulk RNA sequencing (*n* = 6 per group, hM3Dq$^{F/F}$ dam x *Gcm1*-Cre$^{+/-}$ sire, GD 14.5). GTP, guanosine 5′-triphosphate.

Up-regulated GO biological process	Fold enrichment (CNO + MitoQ Cre$^+$ versus CNO Cre$^+$)	FDR
GPCR related		
Negative regulation of GTP binding	29.0	0.2
Oxidative stress		
Response to reactive oxygen species	5.0	0.0003
Regulation of response to stress	2.7	3.7×10^{-5}
Vascular		
Positive regulation of vasculature development	3.7	0.04
Other		
Negative regulation of apoptotic process	2.7	0.0001
Positive regulation of epithelial cell differentiation	7.0	0.03

Syncytiotrophoblast-specific Gαq activation elicits maternal cardiovascular phenotypes, and MitoQ ameliorates some of these effects

Next, the consequences of activating Gαq signaling within the syncytiotrophoblast layer upon maternal cardiovascular phenotypes were examined. Hemodynamic parameters were recorded using radiotelemetric blood pressure transducers implanted before pregnancy (Fig. 6A and fig. S24). Average 24-hour mean arterial pressure was higher in the postinjection period within CNO-injected hM3Dq$^+$ pregnancies compared to saline (P = 0.036; Fig. 6B). This rise was driven by both systolic and diastolic components, and average postinjection heart rate remained consistent among groups (Fig. 6B). Increases in pressure during the dark phase appeared to be associated with augmented ambulatory activity (Fig. 6A). However, elevations in mean arterial pressure persisted on GDs in which activity was equivalent or lower in CNO-injected dams, suggesting some degree of hypertension regardless of activity status.

Proteinuria at GD 14.5 was exacerbated in pregnancies subjected to syncytiotrophoblast-specific Gαq induction (P = 0.0031), but this effect was mitigated by cotreatment with MitoQ (P = 0.0006; Fig. 6C). Electron microscopy revealed signs of mild tubular injury but an absence of classic endotheliosis in a representative kidney sample from the CNO-treated cohort (Fig. 6D). Observations included the presence of segmental congestion in peritubular capillaries, occasional endothelial swelling, segmental congestion in glomerular capillaries, and segmental foot process effacement.

Syncytiotrophoblast-restricted Gαq activation led to an elevation in several proinflammatory chemokines, cytokines, and proteinases in the maternal circulation at GD 14.5 that may mediate the induction of hypertension and proteinuria. In particular, there was an increase in plasma matrix metallopeptidase-9 (MMP9), C-X-C motif chemokine ligand 5 (LIX/CXCL5), subunit beta of interleukin-12 (IL12p40), macrophage-derived chemokine (MDC), C-X-C motif chemokine ligand 10 (IP10/CXCL10), monocyte chemotactic protein 5/chemokine (C-C motif) ligand 12 (MCP5/CXCL12), and a numerical rise that was not statistically significant in interleukin-6 (IL6) (Fig. 7A and table S3). Of these, IL12p40 and IL6 were elevated within human preeclamptic plasma and MMP9 in cases with severe features compared to preeclampsia without severe features (Fig. 7B and table S4). Other investigations have associated MDC, IP10, and MCP5 with preeclampsia (*60*, *61*) or gestational hypertension (*60*), whereas LIX and MMP9 have been implicated in related phenotypes, such as resistant albuminuria (*62*), endothelial dysfunction (*63*), early pregnancy failure (*64*), and leukocytosis (*65*, *66*). MitoQ coadministration suppressed circulating LIX, IL20p40, and MDC and increased tissue inhibitor of matrix metalloproteinases-1 (TIMP-1), an inhibitor of MMP-9 (Fig. 7A and table S3) (*67*).

Administration of CNO did not increase maternal plasma sFLT1 (P = 0.18; Fig. 7C). Our interpretation was confounded, however, by differences in the number (i.e., biomass) of Cre$^+$ placentas within individual dams. Within CNO-injected double-transgenic dams, there was a positive correlation between plasma sFLT1 and the number of Cre$^+$ placentas (Pearson R = 0.76, P = 0.006; Fig. 7C). These findings support the ideas that sFLT1 is primarily placenta derived and that it is positively regulated by Gαq signaling in the syncytiotrophoblast. Last, coadministration of MitoQ suppressed circulating sFLT1 (P = 0.036; Fig. 7C), again indicating that

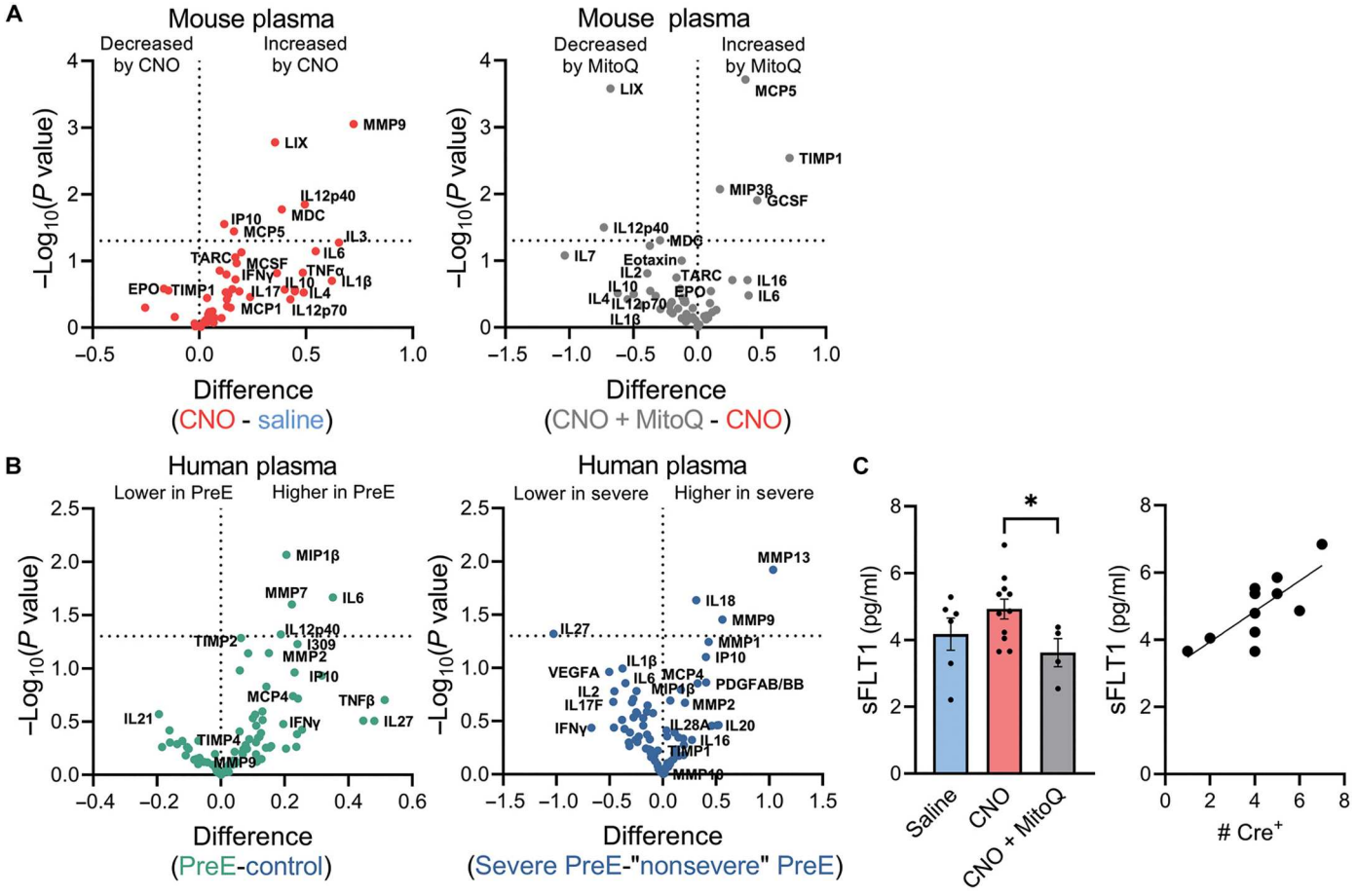

Fig. 7. Maternal circulating factors altered in mouse model of syncytiotrophoblast-specific Gαq signaling (*hM3Dq*$^{F/F}$ dam x *Gcm1*-Cre$^{+/-}$ sire, GD 14.5) and human preeclampsia. (**A**) Levels within mouse plasma (saline $n = 5$, CNO $n = 11$, CNO + MitoQ $n = 3$). (**B**) Levels within human plasma during pregnancy (control $n = 10$, PreE $n = 10$, severe PreE = 6, "nonsevere" PreE $n = 4$). (**C**) Mouse plasma sFLT1 and correlation to the load of Cre^{+} placentas within CNO-injected double-transgenic pregnancies. Each datapoint represents a biological replicate; *$P < 0.05$, multiple unpaired *t* tests (two-tailed) or one-way ANOVA with Bonferroni multiple comparisons procedure.

syncytiotrophoblast Gαq-mediated induction of this well-recognized biomarker and mechanistic contributor of preeclampsia is dependent on oxidative stress.

DISCUSSION

The current study provides critical experimental evidence testing and supporting the concept that the accumulation of syncytiotrophoblast stress plays a causal role in the development of preeclampsia. Further, our findings build upon this theory to suggest that excess Gαq signaling perpetuates this stress and the resultant maternal-fetal aberrations, which are in part mediated by an imbalanced redox state (Fig. 8). This research provides etiological insight regarding a cause of syncytiotrophoblast dysfunction and adds to the growing body of literature supporting the therapeutic utility of targeting oxidative stress to slow the progression of preeclampsia.

Data reported here provide evidence of enhanced Gαq-modulated second messenger propagation in human syncytiotrophoblasts during preeclampsia, illustrated by increased PLCβ protein. We suspect that this effect is a result of excess input from hormones (vasopressin, angiotensin II, and endothelin-1) or placental loss of *RGS2*, an endogenous buffer of Gαq signaling, as these mechanisms are already implicated in preeclampsia pathogenesis by our team and others (*25*, *26*, *30*, *68*). Although studies confirm the presence of *RGS2* and various Gαq-coupled receptors in human syncytiotrophoblast cells (*69*–*71*), we did not attempt to empirically decipher the precise cause of elevated PLCβ in our human placental samples. Single-cell RNA sequencing by Zhang *et al.* (*72*) demonstrated an enrichment of genes pertaining to calcium-dependent protein binding in third trimester syncytiotrophoblasts from preeclamptic patients compared to healthy pregnancies. Our analysis of the available gene set (*72*) using Shiny GO Molecular Function terms also revealed up-regulated G protein α subunit binding, both of which allude to the potential involvement of the Gαq pathway (fig. S25). Because the multinucleated nature of syncytiotrophoblasts is not ideal for single-cell RNA sequencing applications (*73*) and this technique provides limited sequencing depth, we chose to complement these data by microdissecting human syncytiotrophoblasts for protein quantification via immunoassay. This approach limited the number of protein targets that could be measured from a single sample but allowed greater sensitivity and bolsters the transcriptomic findings by Zhang *et al.* (*72*).

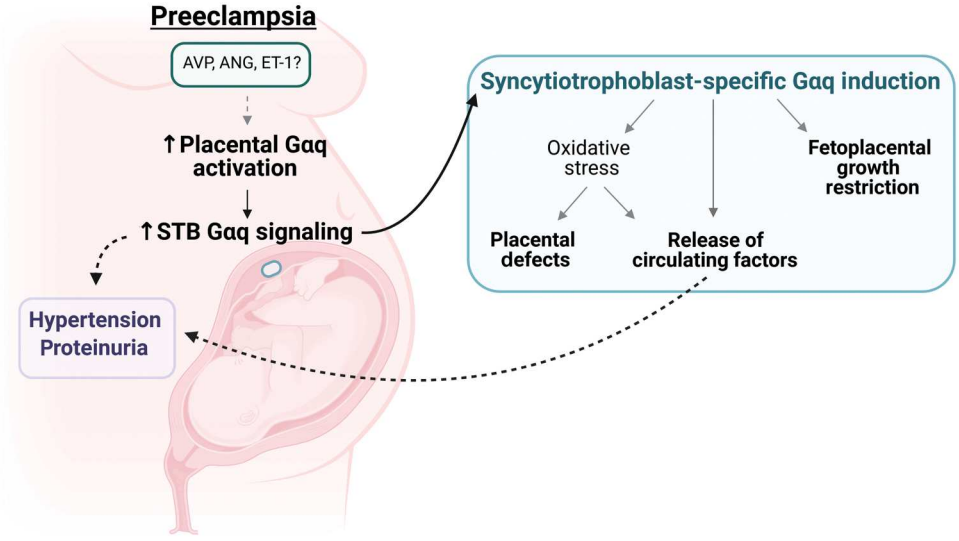

Fig. 8. Working model. Schematic highlights the major experimental findings and illustrates the relationship between excess syncytiotrophoblast Gαq signaling, placental stress, and preeclamptic phenotypes; AVP, vasopressin. ANG, angiotensin II; ET-1, endothelin-1. Image was created using BioRender (www.biorender.com).

A body of literature links Gαq acting hormones and a lack of GPCR inhibitory proteins to placental oxidative stress and mitochondrial dysfunction in animal models (*25*, *26*, *31*, *32*). Mitochondria are a major producer of the oxygen free radical superoxide, whereby electrons escape the canonical transfer system within the electron transport chain and react with molecular oxygen (*74*). In excess, superoxide and its by-products promote detrimental oxidation reactions (*75*, *76*) that contribute to DNA mutations (*77*), impaired protein folding (*78*), altered ion transport (*79*), apoptosis (*78*, *80*), and necrosis (*80*), which can impair placental capacity (*76*). Thus, SOD2 defends against superoxide modulated impairments by converting superoxide to hydrogen peroxide within the mitochondrial matrix (*50*), but its catalytic abilities can be overwhelmed in states of high oxidative stress. Preeclamptic human syncytiotrophoblasts exhibit signs of oxidative damage and impaired respiratory capacity (*16*–*18*), and here we demonstrate elevated SOD2 and lipid peroxidation. Simultaneously, these observations suggest that the rise in SOD2 is a compensatory yet insufficient adaptation to overcome the antioxidant demands imposed by the preeclamptic milieu, but the relationship to Gαq signaling had not been established within the context human preeclampsia or trophoblast subtypes. Notably, our data begins to address this gap and demonstrates a significant positive association among PLCβ and SOD2 in human syncytiotrophoblasts.

Although the precise mechanisms linking Gαq activation and mitochondrial-derived superoxide production have yet to be elucidated within this syndrome, it can be postulated that the connection between pathways involves the Gαq messenger, PKC, and its interactions with NADPH oxidase (NOX), a cellular enzyme responsible for the generation of superoxide (*81*). Several studies have identified PKC as a positive regulator of NOX whereby PKC exerts its effects by phosphorylating NOX subunits (*82*, *83*). Of the many NOX isoforms, NOX2 has been shown to promote reverse electron transfer in response to angiotensin II and therefore contributes to the formation of mitochondrial-derived superoxide (*84*). Studies suggest that MitoQ is a substrate for respiratory complex II and thereby eliminates the burden of backflow of electrons from complex II to I (*85*, *86*).

Complementing our human discoveries regarding the potential relationship between enhanced Gαq signaling and oxidative stress within the syncytiotrophoblast layer during preeclampsia, we took advantage of transgenic mice to assess the direct effects of selective activation of the Gαq cascade only within this cell type. Previous publications by our lab implicate placental GPCR signaling to the development of preeclamptic phenotypes via elevated circulating vasopressin (*26*, *30*) or heterozygous loss of placental *Rgs2* (*35*). These models are confounded by the actions of vasopressin and *Rgs2* on many cells and receptor subtypes within and outside the placenta and do not specifically address the role of Gαq or the syncytiotrophoblast stress hypothesis. However, many of the morphological and molecular changes reported in those studies were similar to those observed here with the exception of placental hypoxia, which was not detected following vasopressin infusion or reduced placental *Rgs2*. We are left to hypothesize that gestational age, crosstalk among G protein pathways, the strength, timing, duration of G protein activation, and the varied actions of these stimulants upon distinct neighboring cell types may all contribute to the discordant induction of hypoxia within these investigations.

The labyrinth layer of mouse placenta contains two distinct, but functionally similar, populations of syncytiotrophoblast, responsible for mediating the passage of substances between maternal blood sinusoids and fetal capillaries (*73*). The current manipulation was limited to syncytiotrophoblast II cells, located in closest proximity to the fetal vasculature. Thus, it is logical that there was diminished labyrinth CD31 staining, denoting a decrease in fetal capillarization, which may have partially driven the fetal growth restriction. With regard to other vascular effects, mouse decidual spiral arteries undergo structural remodeling from GD 7.5 to 10.5 to allow greater oxygen transfer (*87*), but their vascular reactivity to vasoactive agonists is retained (*88*). Therefore, the reduced spiral artery diameter following hM3Dq activation in syncytiotrophoblast II cells from GD 12.5 to 14.5 was likely a consequence of factors

released from the syncytium into maternal circulation rather than incomplete remodeling. Overall, the histologic abnormalities present upon syncytiotrophoblast-localized Gαq stimulation suggest potential uteroplacental dysfunction, which contributes to hypoxia, inadequate nutrient delivery, and subsequent fetal growth restriction (*89*) and preeclampsia.

It is profound that stimulation of a single second messenger cascade in one subset of syncytiotrophoblasts is sufficient to augment proteinuria and blood pressure in the mother. We speculate that these physiologic effects were a result of altered signaling, placental secretions, and trophoblast damage. While the maternal phenotypes are significant but not severe, it should be noted that only ~50% of placentas within a dam were affected, which lessens the "biomass" or "load" of syncytiotrophoblast stress signals. Acknowledging the lack of a large hypertensive effect, blood pressure was not evaluated in the double-transgenic dams receiving concurrent CNO and MitoQ. However, a previous study confirmed that MitoQ supplementation beginning at GD 13.5 diminished the rise in maternal systolic blood pressure in a modified reduced uterine perfusion pressure mouse model of preeclampsia (*22*). Future studies are warranted to determine whether more intense or continuous activation of hM3Dq, in the syncytiotrophoblast or other layers and during different gestational age ranges, would elicit a much greater blood pressure phenotype—and if this requires the induction of oxidative stress.

The placenta is known to release bioactive factors and syncytiotrophoblast-derived extracellular vesicles into the maternal circulation (*19*), and syncytiotrophoblasts are a predominant storage site for sFLT1 (*90*). Therefore, the systemic maternal effects following syncytiotrophoblast-localized Gαq stimulation are presumably attributed to changes in circulating chemokines, cytokines, and sFLT1. There is a convergence of pathways that link Gαq signaling, oxidative stress, and inflammation that may explain the results of the current investigation. As mentioned, the Gαq effector, PKC, mediates phosphorylation events to activate NOX and increase intracellular superoxide (*82*–*84*). PKC and superoxide independently promote activation of nuclear factor κB (NF-κB) (*91*, *92*), a well-established transcription factor involved in the regulation of inflammatory responses (*93*). Preeclamptic placentas exhibit greater NF-κB staining, much of which is localized to syncytiotrophoblast cells (*93*). Many of the maternal plasma immune markers augmented in the current study are established or predicted NF-κB target genes, including IL12p40 (*94*), LIX (*95*), MMP9 (*96*), and IP10 (*97*). Recognizing increased placental PKC and reactive oxygen species are relevant in our experimental mouse model and have been previously linked to NF-κB mobilization (*91*–*93*), it is plausible that these circulating inflammatory mediators are placentally derived. Further, MitoQ can cross the rodent placenta (*22*, *98*) to locally scavenge free radicals. Therefore, the reductions in plasma IL12p40 and LIX within the CNO + MitoQ cohort suggest that these NF-κB–responsive elements may be perpetuated by oxidative stress.

As alluded to, the primary limitations of this study relate to the severity of insult permitted within the syncytiotrophoblast-specific model as only a fraction of placentas within a dam expressed the hM3Dq receptor, and the *Gcm1* Cre driver only targets one of the two syncytiotrophoblast layers. Unfortunately, the current availability (and lack thereof) of cell-specific Cre driver strains does not allow manipulations of both syncytiotrophoblast I and II cells. Further, the short injection period was chosen to avoid DREADD desensitization but may have hindered the acceleration of placental stress. While we would have preferred a more thorough and broad characterization of human and mouse syncytiotrophoblasts, these cells form a large, continuous multinucleated surface layer that is difficult to directly isolate and profile using single-cell omics approaches. Human syncytiotrophoblasts can be differentiated from cytotrophoblasts in cell culture; however, this removes them from their natural environment and prevents integrated explorations, as preeclampsia is a systemic disorder.

Emerging technologies using peptide-coated nanoparticles can be used to deliver cargo to the syncytiotrophoblast layer in human placental explants (*99*) and could be leveraged for site-specific targeting of drugs to dampen Gαq activation. MitoQ supplementation is a simpler option and provides protection in the present study and other animal models of preeclampsia (*22*, *98*, *100*), validating its efficacy in many diverse subtypes of the disorder. MitoQ is already available in a stable formulation for oral dosing and has been administered to humans with no severe adverse events (*101*), making it a reasonable candidate for translation to the clinic. Future work would require honing in on the population of patients most amenable to MitoQ treatment, the ideal time of administration, dosing, and monitoring of pregnancy outcomes.

In summary, excess Gαq signaling in the syncytiotrophoblast layer is sufficient to cause pathological features of preeclampsia via a mechanism involving mitochondrial reactive oxygen species. Our findings support the wide array of correlative human data, suggesting that syncytiotrophoblast stress has a substantial role in the development of this serious disorder (*19*) and identifies Gαq signaling and reactive oxygen species as a targetable source of this stress. This additional mechanistic insight may be beneficial for the advancement of treatment options and health outcomes within affected women and their children as preeclampsia remains largely unsolved (*102*).

MATERIALS AND METHODS

Experimental design

The objectives of this study were to determine the causality of syncytiotrophoblast stress in preeclampsia and to explore Gαq signaling as an etiologic factor. Our human experiments demonstrating enhanced Gαq-related activity in villous placenta and syncytiotrophoblast cells during preeclampsia led to our mouse breeding paradigms for fetoplacental (*hM3Dq*$^{F/F}$ dam x *Actb*-Cre$^{+/+}$ sire) and syncytiotrophoblast-specific (*hM3Dq*$^{F/F}$ dam x *Gcm1*-Cre$^{+/-}$ sire) Gαq induction. Further, the association between Gαq-related and mitochondrial antioxidant proteins in human syncytiotrophoblasts led to the additional cohort of mice receiving MitoQ within the syncytiotrophoblast-specific model. The sample sizes for experiments using human tissue were determined by the availability of tissue. For murine experiments, sample sizes were calculated using effect sizes and variance from our previous studies (*26*, *30*, *35*) ($\alpha = 0.05$ and $\beta = 0.2$). Injections were randomly assigned among each round of timed pregnancies. Molecular assays and histological assessments were performed in a blinded manner. $n = 1$ CNO-injected animal subject (*hM3Dq*$^{F/F}$ dam x *Gcm1*-Cre$^{+/-}$ sire) was discarded from analyses because the dam carried no Cre^{+} fetoplacental units.

Human samples

Institutional Review Board approval and written informed consent were granted before the use of any human specimens. Consented plasma and placental samples and associated clinical data (tables S5 and S6) were procured from the Medical College of Wisconsin Maternal Research Placenta and Cord Blood Bank. Preeclampsia was diagnosed on the basis of the presence of hypertension ≥ 140 mmHg (systolic) or ≥ 90 mmHg (diastolic) on two occasions after 20 weeks of gestation and end organ damage. Preeclampsia with severe features indicates any of the following: blood pressure ≥ 160 mmHg (systolic) or ≥ 110 mmHg (diastolic), thrombocytopenia, impaired liver function, renal insufficiency, pulmonary edema, or neurological symptoms. Control samples were obtained from pregnancies that were not affected by chronic hypertension, gestational hypertension, preeclampsia, or gestational diabetes.

Animal subjects

Animal procedures were approved by the Medical College of Wisconsin Institutional Animal Care and Use Committee. Mice were originally obtained from Jax labs (*Cag*-FLEX-*hM3Dq*, 026943; *Gcm1*-Cre, 026943; *Actb*-Cre, 033984; C57BL/6J, 000664). All mice were housed in a temperature and humidity-controlled facility with ad libitum access to 2029× Teklad diet and water. Male and female mice were housed together for a single overnight mating to ensure accurate assessment of GD. The light cycle following copulation was deemed GD 0.5. Pregnant dams received intraperitoneal injections (CNO 2 mg/kg body weight; MitoQ 5 mg/kg body weight; saline 2 ml/kg body weight) within the first half of the light cycle once daily from GD 12.5 to 14.5. Dams were euthanized by CO_2 asphyxiation and subsequent decapitation a minimum of 1 hour following the injection on GD 14.5 for collection of maternal tissues, plasma, and fetoplacental units.

PLC activity assay

PLC activity was evaluated in villous placental tissue using a colorimetric assay (Abcam, ab2773343). Briefly, 0.1 ± 0.2 g (mean ± SEM) of sample was homogenized in 200 μl assay buffer using a pestle and centrifuged at 10,000*g* at 4°C for 20 min. Two microliters of the supernatant was added per reaction. Absorbance was measured at 405 nm every 41 s for 60 min. Activity was calculated on the basis of product generated within the linear portion of each reaction using a standard curve.

Laser capture microdissection

For downstream processing of proteins, frozen human placental specimens were sectioned at 8 μm on a Leica CM1950 Cryostat that underwent prior ultraviolet (UV) disinfection and cleaning with 100% ethanol. Samples were mounted on polyethylene naphthalate (PEN) membrane glass slides (Carl Zeiss, 15350731) pretreated with UV radiation and 70% ethanol and transiently stored on dry ice for subsequent preparation. Sections were then dipped in cold 70% ethanol for 30 s followed by staining with hematoxylin solution containing 1 μM phenylmethylsulfonyl fluoride (Thermo Fisher Scientific, 36978) and 50× Roche cOmplete protease inhibitor cocktail (Sigma-Aldrich, 11697498001) for 30 s. Hematoxylin was washed by immersion in distilled ultrapure water (Invitrogen, Thermo Fisher Scientific, 10977015) containing 1 μM phenylmethylsulfonyl fluoride and 50× Roche cOmplete protease inhibitor cocktail, twice. Slides were further dehydrated and cleared in 70% ethanol for 30 s, 100% ethanol for 1 min, xylene for 5 min, and fresh xylene for 5 more minutes before brief drying in a chemical hood. Syncytiotrophoblast capture occurred on a Zeiss Palm Microbeam Laser Microdissection system. Regions of interest were identified and outlined using a 40× objective on a motorized inverted microscope or subsequent UV laser cutting at the minimum power necessary to penetrate the tissue and catapulting onto an adhesive cap (Carl Zeiss, 10138374) for 60 min.

Protein expression

Ten microliters of radioimmunoprecipitation assay buffer containing 1 mM phenylmethylsulfonyl fluoride and 1× Roche cOmplete protease inhibitor cocktail was immediately pipetted onto the collected human syncytiotrophoblast cells and placed on ice for 30 min. Fractions were vortexed, centrifuged, and stored at −80°C. PLCβ1 and PLCβ3 are the most highly expressed isoforms within human syncytiotrophoblast (*69*, *71*) and therefore were probed using a recombinant antibody that detects both isoenzymes. Protein expression of PLCβ1/3 (Abcam, recombinant rabbit monoclonal antibody, ab184743, 1:100), SOD2 (Cell Signaling, rabbit monoclonal antibody, #13194, 1:200), and MDA (Abcam, rabbit polyclonal antibody, ab27642, 1:100) were assessed using Simple Western Jess automated capillary–based Western blot system. Protein Simple Chemiluminescence immunoassays were performed according to manufacturer's instructions using replex reagent for total protein detection. Target protein expression was quantified in Compass for SW (6.1.0) and normalized to 50,000 U of total protein or β-actin [ACTB (Abcam, Rabbit polyclonal antibody), ab8227, 1:100].

For downstream processing of mRNA, frozen human placental specimens were sectioned at 6 μm on a Leica CM1950 cryostat. All surfaces were precleaned with 100% ethanol, and removable cryostat parts were treated with ribonuclease (RNase) zap before sectioning. Samples were mounted on UV-exposed PEN membrane glass slides (Thermo Fisher Scientific, LCM0522) and stored at −80°C for future use. Preceding dissection, sections were dipped in chilled 95% ethanol for 30 s and stained with chilled cresyl violet solution (Abcam, ab246817) for 20 s, followed by immersion in 75% ethanol for 20 s, 95% ethanol for 30 s, 100% ethanol for 30 s three times, xylene for 30 s twice, and xylene for 5 min. Slides were air-dried in a chemical hood before collection using an Arcturus XT Laser Capture Microdissection System. Portions of the syncytiotrophoblast layer were identified and outlined using a 40× objective on a motorized inverted microscope. These areas were attached to an adhesive cap (Thermo Fisher Scientific, Applied Biosystems, LCM0211) with an infrared laser and separated from surrounding tissue via UV laser cutting for a maximum of 60 min.

Quantitative real-time polymerase chain reaction

An RNeasy Micro Kit (Qiagen, 74004) was used for RNA extraction according to the recommended protocol with minor modifications. Adjustments included adding Recombinant RNase Inhibitor (Takara, 2313A) to the supplied lysis buffer solution rather than 2-mercaptoethanol. Microdissected cells were immediately lysed with 350 μl of lysis buffer containing 5 μl (200 U, 40 U/μl) of RNase inhibitor, centrifuged, and stored at −80°C. Upon rapid thawing in a water bath, 5 μl (200 U) of RNase inhibitor was added to samples again, and RNA was extracted with on-column deoxyribonuclease (DNase) digestion for 15 min. RNA was eluted

in 12 μl of RNase-free water. Quantity and quality were assessed using fragment analysis and on a NanoDrop (Thermo Fisher Scientific, NanoDrop One). RNA was reverse-transcribed to cDNA using the SuperScript VILO cDNA Synthesis Kit (Thermo Fisher Scientific, Invitrogen, 111754) and amplified using TaqMan PreAmp Master Mix according to the manufacturer's protocol. Briefly, TaqMan gene expression assay for human *GAPDH* (Thermo Fisher Scientific, Hs02786624_g1, 4453320, FAM-MGB), *SOD2* (Thermo Fisher Scientific, Hs00167309_m1, 4453320, FAM-MGB), and *ITPR3* (Thermo Fisher Scientific, Hs01573539_m1, 4448892, FAM-MGB) were pooled into a reaction containing TaqMan PreAmp Master Mix and cDNA and then preamplified on a thermal cycler for 14 cycles. Quantitative real-time polymerase chain reaction (PCR) was performed on amplified product using TaqMan Gene Expression Assays using an Applied Biosystems Step One Plus Real-Time PCR instrument (Thermo Fisher Scientific). Gene expression was analyzed via the Livak method (*103*).

Preparation of injected drugs

CNO (Tocris, 4935) was dissolved in 0.9% saline at a concentration of 0.5 μg/μl on the first day of injections and stored at 4°C between days. MitoQ (Focus Biomolecules, 10-1363) was dissolved to stock solution (70 mg/ml) in dimethyl sulfoxide and stored at −20°C. Stock solution was diluted daily in 0.9% saline to 1 μg/μl.

Placental histology

All placentas were rinsed in phosphate-buffered saline (PBS), grossly sectioned in half, and drop fixed in 10% neutral buffered formalin. After 48 hours, placentas were transferred to 70% ethanol before routine paraffin embedding, sectioning at 4 μm, and hematoxylin and eosin staining by the Medical College of Wisconsin Children's Research Institute histology core. Stitched images were created at ×20 magnification on a Keyence BZ-X series microscope for counting of decidual spiral arteries. The luminal diameter of spiral arteries and layer thickness were examined in ImageJ. All spiral arteries were measured and averaged for each placenta. Each placental layer was measured in the thickest region perpendicular to the base of the placenta. Investigator was blinded to treatment group when performing histological measurements.

CD31 immunohistochemistry

CD31 detection occurred using a Cell Signaling reagent system. Unstained 4-μm paraffin-embedded placental sections were deparaffinized and rehydrated in a series of xylene, ethanol, and water washes before citrate treatment (Cell Signaling, 14746) for antigen unmasking. Samples were blocked with 3% hydrogen peroxide for 10 min and 5% normal goat serum (Cell Signaling, 5425) in tris-buffered saline with Tween 20 (Cell Signaling, 9997) for 1 hour. CD31 rabbit monoclonal antibody (Cell Signaling, 77699, 1:100) in antibody diluent (Cell Signaling, 8112) was applied and incubated overnight at 4°C. Horseradish peroxidase SignalStain Boost Detection Reagent for rabbit immunoglobulin G (Cell Signaling, 8114) and diaminobenzidine (DAB) substrate (Cell Signaling, catalog no. 8059) were used for CD31 staining. Slides were counterstained in hematoxylin, dehydrated, and mounted for imaging on a Keyence BZ-X series microscope. Stitches (20×) of the entire placenta were analyzed via color deconvolution and area quantification in ImageJ.

Murine placental protein expression

Layer-enriched tissue dissection of murine placenta was performed as outlined by Qu *et al.* (*104*). Briefly, uterine muscle and chorionic plate were removed before separating the junctional zone from the underlying labyrinth, which is characterized by a dark red appearance. Techniques were previously validated using quantitative PCR for layer-specific markers (decidua: *Lgals3*, spongiotrophoblast: *Tpbpa*, syncytiotrophoblast II: *Gcm1*). Whole thickness placental or labyrinth dissections were rinsed in cold PBS and then transferred to a microcentrifuge tube on ice containing 200 μl of cell lysis buffer (Thermo Fisher Scientific, Invitrogen, FNN0011) prepared with 1× Roche cOmplete protease inhibitor and 1 mM phenylmethylsulfonyl fluoride. Samples were incubated on ice for 30 min, homogenized with a disposable pestle, and centrifuged at 10,000*g* for 10 min at 4°C. The supernatant was transferred to a new tube for protein quantification using the Pierce BCA Protein Assay Kit (Thermo Fisher Scientific, 23227). SOD2 (Cell Signaling, rabbit monoclonal antibody, 13194, 1:200), catalase (Cell Signaling, rabbit polyclonal antibody, 14097, 1:200), and MDA (Abcam, rabbit polyclonal antibody, ab27642, 1:100) protein levels were assessed via Protein Simple Chemiluminescence immunoassay on a Wes automated capillary–based Western blot system and normalized to ACTB (Abcam, rabbit polyclonal antibody, ab8227, 1:100). Expression was quantified in Compass for SW (6.1.0). VEGFA (Thermo Fisher Scientific, Invitrogen, EMVEGFACL) and PlGF (Thermo Fisher Scientific, Invitrogen, EMPGF) were measured per commercially available enzyme-linked immunosorbent assays (ELISAs).

HIF1α protein localization

Cytoplasmic and soluble nuclear protein fractions of whole-thickness mouse placenta were isolated using a Subcellular Protein Fractionation Kit for Tissues (Thermo Fisher Scientific, 87790) and quantified with the Pierce BCA Protein Assay Kit. HIF1α (Abcam, recombinant rabbit monoclonal antibody, ab179483, 1:50) was probed through Protein Simple Chemiluminescence immunoassay on a Wes instrument and normalized to ACTB (Abcam, Rabbit polyclonal antibody, ab8227, 1:100) for cytoplasmic fraction and HDAC1 (Novus Biologicals, rabbit polyclonal antibody, NB10056340SS, 1:200) for soluble nuclear fraction. Quantification occurred in Compass for SW (6.1.0).

Urine protein

Twenty-four–hour urine samples were collected from metabolic cages, as previously (*26*, *35*). Urine was diluted 1:100 and protein content was determined using the Pierce BCA Protein Assay Kit. Concentration (milligrams per milliliter) was calculated in reference to the standard curve. Total daily protein excretion (milligrams per day) was established by multiplying concentration (milligrams per milliliter) by the volume of urine collected.

Electron microscopy

Peripheral regions of fresh kidney and flash-frozen placenta were minced into approximately 1-mm squares and transferred to glutaraldehyde for 48 hours at 4°C. Tissue was then washed in sodium cacodylate buffer three times for 15 min each and stored in sodium cacodylate buffer at 4°C. Further processing and imaging were conducted by the Medical College of Wisconsin Electron Microscopy Core using a JEOL 2100 transmission electron microscope equipped with an ultrahigh-resolution digital camera. Images were

interpreted by a board-certified veterinary pathologist and a renal pathologist.

RNAscope

Chromogenic duplex RNAscope-based in situ hybridization was performed on paraffin-embedded 4-μm placental sections (Advanced Cell Diagnostics, 322430). Sections were baked, deparaffinized, and pretreated with hydrogen peroxide, target retrieval agent, and protease plus. Following, double Z oligo probes for RNA targets were hybridized (*Gcm1*, 429661; *Cre*, 312281) before storage in 5× SSC buffer overnight at room temperature. Probes were then amplified and detected before counterstaining, mounting, and evaluation on a Keyence BZ-X series microscope.

Florescent imaging

Frozen placenta was sectioned at 10 μm on a Leica CM1950 Cryostat and cover-slipped with ProLong Diamond Antifade Mountant with 4′,6-diamidino-2-phenylindole (Thermo Fisher Scientific, Invitrogen, P36966). Stitched images of fluorophores were captured at 10× on a Keyence BZ-X and a Nikon ECLIPSE 80i microscope. Insets were acquired at 100× on a Nikon A1 laser scanning confocal microscope.

Profiling of maternal circulating factors

Circulating maternal immune and cardiovascular markers were detected with Eve Technologies (Calgary) multiplex assays. Undiluted human and mouse plasma was sent for Human Cytokine/Chemokine 71-Plex Discovery Assay (HD71), Human MMP and TIMP Discovery Assay (HMMP/TIMP-S,P), and Mouse Cardiovascular Disease Panel 1 7-Plex Discovery Assay Array (MDCVD1), and plasma was diluted 1:1 in PBS for Mouse Cytokine/Chemokine 44-Plex Discovery Assay Array (MD44). Arrays consisted of fluorescent beads coupled to capture antibodies and biotinylated detection antibodies bound to streptavidin-phycoerythrin conjugate. Identification of analyte was enabled by a dual-laser flow cytometry bead analyzer. Raw data were log-transformed for plotting and statistical comparisons. sFLT1 within mouse plasma was measured via commercially available ELISA (MyBioSource, MBS161443).

Blood pressure by radiotelemetry

Blood pressure and heart rate were recorded by radiotelemetry as described (*26*, *35*, *105*). Radiotelemetric probes (DSI TA11PA-C10) were implanted into the common carotid artery under ketamine/xylazine anesthesia followed by two doses of postprocedure meloxicam. Mice were allowed 1 week to recover after surgery and another week to acclimate to the telemetry suite. Male and female mice were then housed together for a single overnight mating and remated weekly until successful pregnancy was achieved. Pregnancy data were collected at 2000 Hz from GD 11.5 until euthanasia. Continuous recordings were taken 2 hours before injection and 5 hours postinjection. All other recordings were on a 10 min/hour schedule. Dams were initially euthanized at GD 17.5, but this was adjusted to GD 16.5 due to frequent early delivery.

RNA sequencing

Placental transcriptomes were examined by RNA sequencing at GD 14.5; normalized transcript count data have been submitted to the National Center for Biotechnology Information Gene Expression Omnibus (GSE221732) and raw sequence to the Short Read Archive. Frozen placenta was homogenized in 1 ml of TRIzol with 1.4-mm ceramic beads (PerkinElmer, SKU 19-627) on a Bead Mill Mini Homogenizer (Thermo Fisher Scientific, 15-340-164) before the addition of 200 μl of chloroform. Samples were then vortexed for 15 s, incubated at room temperature for 3 min, and centrifuged at 14,000*g* for 15 min at 4°C. Aqueous phase was extracted and combined with an equal volume of 70% ethanol, vortexed, and transferred to a spin column from a PureLink RNA mini kit (Thermo Fisher Scientific, Invitrogen, 12183018A). RNA was extracted in concordance with the provided protocol, including PureLink DNase treatment (Thermo Fisher Scientific, Invitrogen, 12185010). Total RNA was submitted to the Medical College of Wisconsin Mellowes Center for Genomic Sciences and Precision Medicine for bulk RNA sequencing. Briefly, RNA was quantified on a Qubit fluorometer and then evaluated for quality using RNA integrity number (RIN) (9.6 ± 0.1) and percentage of RNA fragments > 200 nucleotides (DV200) (90 ± 0.2) on a fragment analyzer. Libraries were generated with a Takara low input SMART-Seq Stranded preparation kit and underwent quality control through Kapa Quantification and a MiSeq 50 cycle run, and 100-bp paired-end sequencing was performed on a NovaSeq platform with a 200-cycle SP flow cell and a targeted sequence depth of 55 million reads per sample (table S7).

Transcriptomic data analysis

The quality of prealigned data was computed by FastQC. All samples had a median per base sequence quality score above 30, and the average quality per read was 31 (with a value of 27 equating to a 0.2% error rate). Reads were aligned to the Gencode vM23 (GRCm38.p6) mouse reference genome with Star and further processed in the MAPRSeq3 workflow to obtain read counts at the gene and exon levels. Aligned data were inspected via RSeQC modules to ensure appropriate quality metrics including coverage uniformity, inner distance between paired reads, and sequencing saturation (fig. S26). Differential gene expression was tested in EdgeR with a pairwise approach comparing: CNO Cre^+ versus saline Cre^-, CNO Cre^+ versus CNO Cre^-, and CNO + MitoQ Cre^+ versus CNO Cre^+. Lists of up-regulated genes ($P < 0.05$, minimum $\log_2$ fold change of 0.23) were input to Shiny GO (versions indicated in text) for enrichment analysis. Pathways with an enrichment false discovery rate of <0.15 were considered.

Statistical analyses

Quantitative physiological and histological data are depicted as mean ± SEM unless indicated. For mouse fetoplacental assessments, each individual datapoint represents a separate pregnancy. Experimental results for continuous variables were tested for normality and equal variance. Parametric data were analyzed by *t* test (two-tailed) or analysis of variance (ANOVA) followed by Bonferroni correction for multiple comparisons and nonparametric data by Mann-Whitney *U* test using GraphPad Prism 9.5.0. $P < 0.05$ was used as the threshold for significance. Differences in the distribution of categorical variables between groups were assessed by χ^2 test.

Supplementary Materials

This PDF file includes:

Fig. S1 to S26

Tables S1 to S7

REFERENCES AND NOTES

1. L. M. Amaral, M. W. Cunningham Jr., D. C. Cornelius, B. LaMarca, Preeclampsia: Long-term consequences for vascular health. *Vasc. Health Risk Manag.* **11**, 403–415 (2015).
2. S. Rana, E. Lemoine, J. Granger, S. A. Karumanchi, Preeclampsia. *Circ. Res.* **124**, 1094–1112 (2019).
3. M. Lazdam, E. F. Davis, A. J. Lewandowski, S. A. Worton, Y. Kenworthy, B. Kelly, P. Leeson, Prevention of vascular dysfunction after preeclampsia: A potential long-term outcome measure and an emerging goal for treatment. *J. Pregnancy* **2012**, 704146 (2012).
4. S.-W. Cheng, H.-C. Chou, K.-I. Tsou, L.-J. Fang, P.-N. Tsao, Delivery before 32 weeks of gestation for maternal pre-eclampsia: Neonatal outcome and 2-year developmental outcome. *Early Hum. Dev.* **76**, 39–46 (2004).
5. C. Bushnell, M. Chireau, Preeclampsia and stroke: Risks during and after pregnancy. *Stroke Res Treat* **2011**, 858134 (2011).
6. M. S. Tanner, M.-A. Davey, B. W. Mol, D. L. Rolnik, The evolution of the diagnostic criteria of preeclampsia-eclampsia. *Am. J. Obstet. Gynecol.* **226**, S835–S843 (2022).
7. W. Wang, X. Xie, T. Yuan, Y. Wang, F. Zhao, Z. Zhou, H. Zhang, Epidemiological trends of maternal hypertensive disorders of pregnancy at the global, regional, and national levels: A population-based study. *BMC Pregnancy Childbirth* **21**, 364 (2021).
8. N. A. Cameron, I. Everitt, L. E. Seegmiller, L. M. Yee, W. A. Grobman, S. S. Khan, Trends in the incidence of new-onset hypertensive disorders of pregnancy among rural and urban areas in the United States, 2007 to 2019. *J. Am. Heart Assoc.* **11**, e023791 (2022).
9. S. J. Fisher, Why is placentation abnormal in preeclampsia? *Am. J. Obstet. Gynecol.* **213**, S115–S122 (2015).
10. C. P. Sibley, Treating the dysfunctional placenta. *J. Endocrinol.* **234**, R81–R97 (2017).
11. C. W. Redman; A. C. Staff, Preeclampsia, biomarkers, syncytiotrophoblast stress, and placental capacity. *Am. J. Obstet. Gynecol.* **213**, S9.e1 (2015).
12. Y. Wang, S. Zhao, in *Vascular Biology of the Placenta*. (Morgan & Claypool Life Sciences), 2010), 2, 1, 98.
13. T. Cindrova-Davies, N. M. E. Fogarty, C. J. P. Jones, J. Kingdom, G. J. Burton, Evidence of oxidative stress-induced senescence in mature, post-mature and pathological human placentas. *Placenta* **68**, 15–22 (2018).
14. S. Guller, Z. Tang, Y. Y. Ma, S. di Santo, R. Sager, H. Schneider, Protein composition of microparticles shed from human placenta during placental perfusion: Potential role in angiogenesis and fibrinolysis in preeclampsia. *Placenta* **32**, 63–69 (2011).
15. A. Jaremek, M. J. Jeyarajah, G. Jaju Bhattad, S. J. Renaud, Omics approaches to study formation and function of human placental syncytiotrophoblast. *Front. Cell Dev.l Biol.* **9**, (2021).
16. H. W. Yung, F. Colleoni, E. Dommett, T. Cindrova-Davies, J. Kingdom, A. J. Murray, G. J. Burton, Noncanonical mitochondrial unfolded protein response impairs placental oxidative phosphorylation in early-onset preeclampsia. *Proc. Natl. Acad. Sci. U.S.A.* **116**, 18109–18118 (2019).
17. Z. K. Zsengellér, A. Rajakumar, J. T. Hunter, S. Salahuddin, S. Rana, I. E. Stillman, S. Ananth Karumanchi, Trophoblast mitochondrial function is impaired in preeclampsia and correlates negatively with the expression of soluble fms-like tyrosine kinase 1. *Pregnancy Hypertens* **6**, 313–319 (2016).
18. C. Chekir, M. Nakatsuka, S. Noguchi, H. Konishi, Y. Kamada, A. Sasaki, L. Hao, Y. Hiramatsu, Accumulation of advanced glycation end products in women with preeclampsia: Possible involvement of placental oxidative and nitrative stress. *Placenta* **27**, 225–233 (2006).
19. C. W. G. Redman, A. C. Staff, J. M. Roberts, Syncytiotrophoblast stress in preeclampsia: The convergence point for multiple pathways. *Am. J. Obstet. Gynecol.* **226**, S907–S927 (2022).
20. T. Fushima, A. Sekimoto, T. Minato, T. Ito, Y. Oe, K. Kisu, E. Sato, K. Funamoto, T. Hayase, Y. Kimura, S. Ito, H. Sato, N. Takahashi, Reduced uterine perfusion pressure (RUPP) model of preeclampsia in mice. *PLOS ONE* **11**, e0155426 (2016).
21. J. K. Crews, J. N. Herrington, J. P. Granger, R. A. Khalil, Decreased endothelium-dependent vascular relaxation during reduction of uterine perfusion pressure in pregnant rat. *Hypertension* **35**, 367–372 (2000).
22. Y. Yang, P. Xu, F. Zhu, J. Liao, Y. Wu, M. Hu, H. Fu, J. Qiao, L. Lin, B. Huang, H. Jin, X. Liu, Y. Zheng, L. Wen, R. Saffery, M. D. Kilby, J. Yan, L. C. Kenny, H. Qi, C. Tong, P. N. Baker, The potent antioxidant MitoQ protects against preeclampsia during late gestation but increases the risk of preeclampsia when administered in early pregnancy. *Antioxid. Redox Signal.* **34**, 118–136 (2021).
23. S. E. Maynard, J. Y. Min, J. Merchan, K. H. Lim, J. Li, S. Mondal, T. A. Libermann, J. P. Morgan, F. W. Sellke, I. E. Stillman, F. H. Epstein, V. P. Sukhatme, S. A. Karumanchi, Excess placental soluble fms-like tyrosine kinase 1 (sFlt1) may contribute to endothelial dysfunction hypertension, and proteinuria in preeclampsia. *J. Clin. Investig.* **111**, 649–658 (2003).
24. J. P. Bridges, J. S. Gilbert, D. Colson, S. A. Gilbert, M. P. Dukes, M. J. Ryan, J. P. Granger, Oxidative stress contributes to soluble fms-like tyrosine kinase-1 induced vascular dysfunction in pregnant rats. *Am. J. Hypertens.* **22**, 564–568 (2009).
25. K. J. Perschbacher, G. Deng, R. A. Fisher, K. N. Gibson-Corley, M. K. Santillan, J. L. Grobe, Regulators of G protein signaling in cardiovascular function during pregnancy. *Physiol. Genomics* **50**, 590–604 (2018).
26. J. A. Sandgren, G. Deng, D. W. Linggonegoro, S. M. Scroggins, K. J. Perschbacher, A. R. Nair, T. E. Nishimura, S. Y. Zhang, L. N. Agbor, J. Wu, H. L. Keen, M. C. Naber, N. A. Pearson, K. A. Zimmerman, R. M. Weiss, N. C. Bowdler, Y. M. Usachev, D. A. Santillan, M. J. Potthoff, G. L. Pierce, K. N. Gibson-Corley, C. D. Sigmund, M. K. Santillan, J. L. Grobe, Arginine vasopressin infusion is sufficient to model clinical features of preeclampsia in mice. *JCI insight* **3**, e99403 (2018).
27. K. Leavey, S. J. Benton, D. Grynspan, J. C. Kingdom, S. A. Bainbridge, B. J. Cox, Unsupervised placental gene expression profiling identifies clinically relevant subclasses of human preeclampsia. *Hypertension* **68**, 137–147 (2016).
28. P. K. Aggarwal, N. Chandel, V. Jain, V. Jha, The relationship between circulating endothelin-1, soluble fms-like tyrosine kinase-1 and soluble endoglin in preeclampsia. *J. Hum. Hypertens.* **26**, 236–241 (2012).
29. N. F. Gant, G. L. Daley, S. Chand, P. J. Whalley, P. C. MacDonald, A study of angiotensin II pressor response throughout primigravid pregnancy. *J. Clin. Invest.* **52**, 2682–2689 (1973).
30. M. K. Santillan, D. A. Santillan, S. M. Scroggins, J. Y. Min, J. A. Sandgren, N. A. Pearson, K. K. Leslie, S. K. Hunter, G. K. D. Zamba, K. N. Gibson-Corley, J. L. Grobe, Vasopressin in preeclampsia: A novel very early human pregnancy biomarker and clinically relevant mouse model. *Hypertension* **64**, 852–859 (2014).
31. J. Brewer, R. Liu, Y. Lu, J. Scott, K. Wallace, G. Wallukat, J. Moseley, F. Herse, R. Dechend, J. N. Martin Jr., B. LaMarca, Endothelin-1, oxidative stress, and endogenous angiotensin II: Mechanisms of angiotensin II type I receptor autoantibody-enhanced renal and blood pressure response during pregnancy. *Hypertension* **62**, 886–892 (2013).
32. G. Fiore, P. Florio, L. Micheli, C. Nencini, M. Rossi, D. Cerretani, G. Ambrosini, G. Giorgi, F. Petraglia, Endothelin-1 triggers placental oxidative stress pathways: Putative role in preeclampsia. *J. Clin. Endocrinol. Metab.* **90**, 4205–4210 (2005).
33. I. Masuho, S. Balaji, B. S. Muntean, N. K. Skamangas, S. Chavali, J. J. G. Tesmer, M. M. Babu, K. A. Martemyanov, A global map of G protein signaling regulation by RGS proteins. *Cell* **183**, 503–521.e19 (2020).
34. S. P. Heximer, N. Watson, M. E. Linder, K. J. Blumer, J. R. Hepler, RGS2/G0S8 is a selective inhibitor of Gqα function. *Proc. Natl. Acad. Sci. U.S.A.* **94**, 14389–14393 (1997).
35. K. J. Perschbacher, G. Deng, J. A. Sandgren, J. W. Walsh, P. C. Witcher, S. A. Sapouckey, C. E. Owens, S. Y. Zhang, S. M. Scroggins, N. A. Pearson, E. J. Devor, J. A. Sebag, G. L. Pierce, R. A. Fisher, A. E. Kwitek, D. A. Santillan, K. N. Gibson-Corley, C. D. Sigmund, M. K. Santillan, J. L. Grobe, Reduced mRNA expression of RGS2 (regulator of G protein signaling-2) in the placenta is associated with human preeclampsia and sufficient to cause features of the disorder in mice. *Hypertension* **75**, 569–579 (2020).
36. O. S. Walker, S. Walker, R. Ragos, M. K. Wong, M. Adam, A. Cheung, S. Raha, Reactive oxygen species from mitochondria impacts trophoblast fusion and the production of endocrine hormones by syncytiotrophoblasts. *PLOS ONE* **15**, e0229332 (2020).
37. A. M. Lyon, J. J. Tesmer, Structural insights into phospholipase C-β function. *Mol. Pharmacol.* **84**, 488–500 (2013).
38. C. Guo, L. Sun, X. Chen, D. Zhang, Oxidative stress, mitochondrial damage and neurodegenerative diseases. *Neural Regen. Res.* **8**, 2003–2014 (2013).
39. B. N. Armbruster, X. Li, M. H. Pausch, S. Herlitze, B. L. Roth, Evolving the lock to fit the key to create a family of G protein-coupled receptors potently activated by an inert ligand. *Proc. Natl. Acad. Sci. U.S.A* **104**, 5163–5168 (2007).
40. N. R. Sciolino, N. W. Plummer, Y. W. Chen, G. M. Alexander, S. D. Robertson, S. M. Dudek, Z. A. McElligott, P. Jensen, Recombinase-dependent mouse lines for chemogenetic activation of genetically defined cell types. *Cell Rep.* **15**, 2563–2573 (2016).
41. S. E. Ander, M. S. Diamond, C. B. Coyne, Immune responses at the maternal-fetal interface. *Science Immunol.* **4**, eaat6114 (2019).
42. J. L. Sones, R. L. Davisson, Preeclampsia, of mice and women. *Physiol. Genomics* **48**, 565–572 (2016).
43. D. F. Manvich, K. A. Webster, S. L. Foster, M. S. Farrell, J. C. Ritchie, J. H. Porter, D. Weinshenker, The DREADD agonist clozapine N-oxide (CNO) is reverse-metabolized to clozapine and produces clozapine-like interoceptive stimulus effects in rats and mice. *Sci. Rep.* **8**, 3840 (2018).
44. J. M. Roberts, A. Rajakumar, Preeclampsia and soluble fms-like tyrosine kinase 1. *J. Clin. Endocrinol. Metab.* **94**, 2252–2254 (2009).
45. M. A. Opichka, M. W. Rappelt, D. D. Gutterman, J. L. Grobe, J. J. McIntosh, Vascular Dysfunction in Preeclampsia. *Cells* **10**, 3055 (2021).
46. L. Woods, V. Perez-Garcia, M. Hemberger, Regulation of placental development and its impact on fetal growth-new insights from mouse models. *Front. Endocrinol.* **9**, 570 (2018).
47. B. M. Wynne, C.-W. Chiao, R. C. Webb, Vascular smooth muscle cell signaling mechanisms for contraction to angiotensin II and endothelin-1. *J. Am. Soc. Hypertens.* **3**, 84–95 (2009).

48. A. Vilborg, M. C. Passarelli, J. A. Steitz, Calcium signaling and transcription: Elongation, DoGs, and eRNAs. *Receptors Clin. Investig.* **3**, e1169 (2016).
49. A. Savina, M. Furlán, M. Vidal, M. I. Colombo, Exosome release is regulated by a calcium-dependent mechanism in K562 cells. *J. Biol. Chem.* **278**, 20083–20090 (2003).
50. J. M. Flynn, S. Melov, SOD2 in mitochondrial dysfunction and neurodegeneration. *Free Radic. Biol. Med.* **62**, 4–12 (2013).
51. S. Gaweł, M. Wardas, E. Niedworok, P. Wardas, Malondialdehyde (MDA) as a lipid peroxidation marker. *Wiad. Lek.* **57**, 453–455 (2004).
52. V. Nadeau, S. Guillemette, L.-F. Bélanger, O. Jacob, S. Roy, J. Charron, Map2k1 and Map2k2 genes contribute to the normal development of syncytiotrophoblasts during placentation. *Development* **136**, 1363–1374 (2009).
53. J. J. Fisher, L. A. Bartho, A. V. Perkins, O. J. Holland, Placental mitochondria and reactive oxygen species in the physiology and pathophysiology of pregnancy. *Clin. Exp. Pharmacol. Physiol.* **47**, 176–184 (2020).
54. A. L. Fowden, A. N. Sferruzzi-Perri, P. M. Coan, M. Constancia, G. J. Burton, Placental efficiency and adaptation: Endocrine regulation. *J. Physiol.* **587**, 3459–3472 (2009).
55. G. L. Semenza, M. K. Nejfelt, S. M. Chi, S. E. Antonarakis, Hypoxia-inducible nuclear factors bind to an enhancer element located 3′ to the human erythropoietin gene. *Proc. Natl. Acad. Sci. U.S.A.* **88**, 5680–5684 (1991).
56. P. Jaakkola, D. R. Mole, Y. M. Tian, M. I. Wilson, J. Gielbert, S. J. Gaskell, A. . Kriegsheim, H. F. Hebestreit, M. Mukherji, C. J. Schofield, P. H. Maxwell, C. W. Pugh, P. J. Ratcliffe, Targeting of HIF-alpha to the von Hippel-Lindau ubiquitylation complex by O_2-regulated prolyl hydroxylation. *Science* **292**, 468–472 (2001).
57. J. A. Forsythe, B. H. Jiang, N. V. Iyer, F. Agani, S. W. Leung, R. D. Koos, G. L. Semenza, Activation of vascular endothelial growth factor gene transcription by hypoxia-inducible factor 1. *Mol. Cell. Biol.* **16**, 4604–4613 (1996).
58. A. Zimna, M. Kurpisz, Hypoxia-inducible factor-1 in physiological and pathophysiological angiogenesis: Applications and therapies. *Biomed. Res. Int.* **2015**, 549412 (2015).
59. Q. D. Nguyen, S. de Falco, F. Behar-Cohen, W. C. Lam, X. Li, N. Reichhart, F. Ricci, J. Pluim, W. W. Li, Placental growth factor and its potential role in diabetic retinopathy and other ocular neovascular diseases. *Acta Ophthalmol.* **96**, e1–e9 (2018).
60. K. Stefańska, M. Zieliński, M. Jankowiak, D. Zamkowska, J. Sakowska, P. Adamski, J. Jassem-Bobowicz, K. Piekarska, K. Leszczyńska, R. Świątkowska-Stodulska, S. Kwiatkowski, K. Preis, P. Trzonkowski, N. Marek-Trzonkowska, Cytokine imprint in preeclampsia. *Front. Immunol.* **12**, 667841 (2021).
61. A. Szarka, J. Rigó, L. Lázár, G. Bekő, A. Molvarec, Circulating cytokines, chemokines and adhesion molecules in normal pregnancy and preeclampsia determined by multiplex suspension array. *BMC Immunol.* **11**, 59 (2010).
62. H. Pulido-Olmo, C. F. García-Prieto, G. Álvarez-Llamas, M. G. Barderas, F. Vivanco, I. Aranguez, B. Somoza, J. Segura, R. Kreutz, M. S. Fernández-Alfonso, L. M. Ruilope, G. Ruiz-Hurtado, Role of matrix metalloproteinase-9 in chronic kidney disease: A new biomarker of resistant albuminuria. *Clin. Sci.* **130**, 525–538 (2016).
63. J. M. Florence, A. Krupa, L. M. Booshehri, T. C. Allen, A. K. Kurdowska, Metalloproteinase-9 contributes to endothelial dysfunction in atherosclerosis via protease activated receptor-1. *PLOS ONE* **12**, e0171427 (2017).
64. R. Nissi, A. Talvensaari-Mattila, V. Kotila, M. Niinimäki, I. Järvelä, T. Turpeenniemi-Hujanen, Circulating matrix metalloproteinase MMP-9 and MMP-2/TIMP-2 complex are associated with spontaneous early pregnancy failure. *Reprod. Biol. Endocrinol.* **11**, 2 (2013).
65. J. Song, C. Wu, X. Zhang, L. M. Sorokin, In vivo processing of CXCL5 (LIX) by matrix metalloproteinase (MMP)-2 and MMP-9 promotes early neutrophil recruitment in IL-1β–induced peritonitis. *J. Immunol.* **190**, 401–410 (2013).
66. B. J. Canzoneri, D. F. Lewis, L. Groome, Y. Wang, Increased neutrophil numbers account for leukocytosis in women with preeclampsia. *Am. J. Perinatol.* **26**, 729–732 (2009).
67. Ł. Charzewski, K. A. Krzyśko, B. Lesyng, Structural characterisation of inhibitory and non-inhibitory MMP-9–TIMP-1 complexes and implications for regulatory mechanisms of MMP-9. *Sci. Rep.* **11**, 13376 (2021).
68. J. A. Sandgren, S. M. Scroggins, D. A. Santillan, E. J. Devor, K. N. Gibson-Corley, G. L. Pierce, C. D. Sigmund, M. K. Santillan, J. L. Grobe, Vasopressin: The missing link for preeclampsia? *Am J Physiol Regul Integr Comp Physiol* **309**, R1062–R1064 (2015).
69. R. Vento-Tormo, M. Efremova, R. A. Botting, M. Y. Turco, M. Vento-Tormo, K. B. Meyer, J. E. Park, E. Stephenson, K. Polański, A. Goncalves, L. Gardner, S. Holmqvist, J. Henriksson, A. Zou, A. M. Sharkey, B. Millar, B. Innes, L. Wood, A. Wilbrey-Clark, R. P. Payne, M. A. Ivarsson, S. Lisgo, A. Filby, D. H. Rowitch, J. N. Bulmer, G. J. Wright, M. J. T. Stubbington, M. Haniffa, A. Moffett, S. A. Teichmann, Single-cell reconstruction of the early maternal–fetal interface in humans. *Nature* **563**, 347–353 (2018).
70. X. Li, M. Shams, J. Zhu, A. Khalig, M. Wilkes, M. Whittle, N. Barnes, A. Ahmed, Cellular localization of AT1 receptor mRNA and protein in normal placenta and its reduced expression in intrauterine growth restriction. Angiotensin II stimulates the release of vasorelaxants. *J. Clin. Invest.* **101**, 442–454 (1998).
71. M. Karlsson, C. Zhang, L. Méar, W. Zhong, A. Digre, B. Katona, E. Sjöstedt, L. Butler, J. Odeberg, P. Dusart, F. Edfors, P. Oksvold, K. von Feilitzen, M. Zwahlen, M. Arif, O. Altay, X. Li, M. Ozcan, A. Mardinoglu, L. Fagerberg, J. Mulder, Y. Luo, F. Ponten, M. Uhlén, C. Lindskog, A single–cell type transcriptomics map of human tissues. *Sci. Adv* **7**, eabh2169 (2021).
72. T. Zhang, Q. Bian, Y. Chen, X. Wang, S. Yu, S. Liu, P. Ji, L. Li, M. Shrestha, S. Dong, R. Guo, H. Zhang, Dissecting human trophoblast cell transcriptional heterogeneity in pre-eclampsia using single-cell RNA sequencing. *Mol. Genet. Genomic Med.* **9**, e1730 (2021).
73. B. Marsh, R. Blelloch, Single nuclei RNA-seq of mouse placental labyrinth development. *eLife* **9**, e60266 (2020).
74. H. P. Indo, H. C. Yen, I. Nakanishi, K. I. Matsumoto, M. Tamura, Y. Nagano, H. Matsui, O. Gusev, R. Cornette, T. Okuda, Y. Minamiyama, H. Ichikawa, S. Suenaga, M. Oki, T. Sato, T. Ozawa, D. K. S. Clair, H. J. Majima, A mitochondrial superoxide theory for oxidative stress diseases and aging. *J. Clin. Biochem. Nutr.* **56**, 1–7 (2015).
75. Y. S. Kim, P. Gupta Vallur, R. Phaëton, K. Mythreye, N. Hempel, Insights into the dichotomous regulation of SOD2 in cancer. *Antioxidants* **6**, 86 (2017).
76. Z. Sultana, K. Maiti, J. Aitken, J. Morris, L. Dedman, R. Smith, Oxidative stress, placental ageing-related pathologies and adverse pregnancy outcomes. *Am. J. Reprod. Immunol.* **77**, e12653 (2017).
77. M. Krajcovicová-Kudlácková, M. Dusinská, M. Valachovicová, P. Blazícek, V. Pauková, Products of DNA, protein and lipid oxidative damage in relation to vitamin C plasma concentration. *Physiol. Res.* **55**, 227–231 (2006).
78. S. Reeg, T. Grune, Protein oxidation in aging: Does it play a role in aging progression? *Antioxid. Redox Signal.* **23**, 239–255 (2015).
79. A. Catalá, M. Díaz, Editorial: Impact of lipid peroxidation on the physiology and pathophysiology of cell membranes. *Front. Physiol.* **7**, 423 (2016).
80. A. Ayala, M. F. Muñoz, S. Argüelles, Lipid peroxidation: Production, metabolism, and signaling mechanisms of malondialdehyde and 4-hydroxy-2-nonenal. *Oxid. Med. Cell. Longev.* **2014**, 360438 (2014).
81. R. Rastogi, X. Geng, F. Li, Y. Ding, NOX activation by subunit interaction and underlying mechanisms in disease. *Front. Cell. Neurosci.* **10**, 301 (2016).
82. B. Shao, U. Bayraktutan, Hyperglycaemia promotes cerebral barrier dysfunction through activation of protein kinase C-β. *Diabetes Obes. Metab.* **15**, 993–999 (2013).
83. W. M. Nauseef, B. D. Volpp, S. McCormick, K. G. Leidal, R. A. Clark, Assembly of the neutrophil respiratory burst oxidase. Protein kinase C promotes cytoskeletal and membrane association of cytosolic oxidase components. *J. Biol. Chem.* **266**, 5911–5917 (1991).
84. S. I. Dikalov, R. R. Nazarewicz, A. Bikineyeva, L. Hilenski, B. Lassègue, K. K. Griendling, D. G. Harrison, A. E. Dikalova, Nox2-induced production of mitochondrial superoxide in angiotensin II-mediated endothelial oxidative stress and hypertension. *Antioxid. Redox Signal.* **20**, 281–294 (2014).
85. Y. O'Malley, B. D. Fink, N. C. Ross, T. E. Prisinzano, W. I. Sivitz, Reactive oxygen and targeted antioxidant administration in endothelial cell mitochondria. *J. Biol. Chem.* **281**, 39766–39775 (2006).
86. A. M. James, M. S. Sharpley, A. R. B. Manas, F. E. Frerman, J. Hirst, R. A. J. Smith, M. P. Murphy, Interaction of the mitochondria-targeted antioxidant MitoQ with phospholipid bilayers and ubiquinone oxidoreductases. *J. Biol. Chem.* **282**, 14708–14718 (2007).
87. A. Elia, F. Charalambous, P. Georgiades, New phenotypic aspects of the decidual spiral artery wall during early post-implantation mouse pregnancy. *Biochem. Biophys. Res. Commun.* **416**, 211–216 (2011).
88. S. Leonard, P. D. A. Lima, B. A. Croy, C. L. Murrant, Gestational modification of murine spiral arteries does not reduce their drug-induced vasoconstrictive responses in vivo. *Biol. Reprod.* **89**, 139 (2013).
89. M. Takahashi, S. Makino, K. Oguma, H. Imai, A. Takamizu, A. Koizumi, K. Yoshida, Fetal growth restriction as the initial finding of preeclampsia is a clinical predictor of maternal and neonatal prognoses: A single-center retrospective study. *BMC Pregnancy Childbirth* **21**, 678 (2021).
90. A. J. Buurma, M. E. Penning, F. Prins, J. M. Schutte, J. A. Bruijn, S. Wilhelmus, A. Rajakumar, K. W. M. Bloemenkamp, S. A. Karumanchi, H. J. Baelde, Preeclampsia is associated with the presence of transcriptionally active placental fragments in the maternal lung. *Hypertension* **62**, 608–613 (2013).
91. Y. H. Yee, S. J. F. Chong, L. R. Kong, B. C. Goh, S. Pervaiz, Sustained IKKβ phosphorylation and NF-κB activation by superoxide-induced peroxynitrite-mediated nitrotyrosine modification of B56γ3 and PP2A inactivation. *Redox Biol.* **41**, 101834 (2021).
92. K. Saijo, I. Mecklenbräuker, A. Santana, M. Leitger, C. Schmedt, A. Tarakhovsky, Protein kinase C β controls nuclear factor κB activation in B cells through selective regulation of the IκB kinase α. *J. Exp. Med.* **195**, 1647–1652 (2002).
93. J. E. Vaughan, S. W. Walsh, Activation of NF-κB in placentas of women with preeclampsia. *Hypertens. Pregnancy* **31**, 243–251 (2012).

94. T. L. Murphy, M. G. Cleveland, P. Kulesza, J. Magram, K. M. Murphy, Regulation of interleukin 12 p40 expression through an NF-κB half-site. *Mol. Cell. Biol.* **15**, 5258–5267 (1995).
95. J. B. Smith, D. J. Wadleigh, Y.-R. Xia, R. A. Mar, H. R. Herschman, A. J. Lusis, Cloning and genomic localization of the murine LPS-induced CXC chemokine (LIX) gene, *Scyb5*. *Immunogenetics* **54**, 599–603 (2002).
96. C. He, Molecular mechanism of transcriptional activation of human gelatinase B by proximal promoter. *Cancer Lett.* **106**, 185–191 (1996).
97. Y. Ohmori, T. A. Hamilton, Cooperative interaction between interferon (IFN) stimulus response element and kappa B sequence motifs controls IFN gamma- and lipopolysaccharide-stimulated transcription from the murine IP-10 promoter. *J. Biol. Chem.* **268**, 6677–6688 (1993).
98. A. M. Nuzzo, E. J. Camm, A. N. Sferruzzi-Perri, T. J. Ashmore, H. W. Yung, T. Cindrova-Davies, A. M. Spiroski, M. R. Sutherland, A. Logan, S. Austin-Williams, G. J. Burton, A. Rolfo, T. Todros, M. P. Murphy, D. A. Giussani, Placental adaptation to early-onset hypoxic pregnancy and mitochondria-targeted antioxidant therapy in a rodent model. *Am. J. Pathol.* **188**, 2704–2716 (2018).
99. A. King, C. Ndifon, S. Lui, K. Widdows, V. R. Kotamraju, L. Agemy, T. Teesalu, J. D. Glazier, F. Cellesi, N. Tirelli, J. D. Aplin, E. Ruoslahti, L. K. Harris, Tumor-homing peptides as tools for targeted delivery of payloads to the placenta. *Sci. Adv.* **2**, e1600349 (2016).
100. K. J. Botting, K. L. Skeffington, Y. Niu, B. J. Allison, K. L. Brain, N. Itani, C. Beck, A. Logan, A. J. Murray, M. P. Murphy, D. A. Giussani, Translatable mitochondria-targeted protection against programmed cardiovascular dysfunction. *Sci. Adv.* **6**, eabb1929 (2020).
101. R. A. Smith, M. P. Murphy, Animal and human studies with the mitochondria-targeted antioxidant MitoQ. *Ann. N. Y. Acad. Sci.* **1201**, 96–103 (2010).
102. A. Conde-Agudelo, R. Romero, SARS-CoV-2 infection during pregnancy and risk of preeclampsia: A systematic review and meta-analysis. *Am. J. Obstet. Gynecol.* **226**, 68–89.e3 (2022).
103. K. J. Livak, T. D. Schmittgen, Analysis of relative gene expression data using real-time quantitative PCR and the $2^{-\Delta\Delta C}_{T}$ Method. *Methods* **25**, 402–408 (2001).
104. D. Qu, A. McDonald, K. J. Whiteley, S. A. Bainbridge, S. L. Adamson, in *The Guide to Investigation of Mouse Pregnancy*, B. A. Croy, A. T. Yamada, F. J. DeMayo, S. L. Adamson, Eds. (Academic Press, 2014), pp. 529–535
105. J. L. Grobe, C. L. Grobe, T. G. Beltz, S. G. Westphal, D. A. Morgan, D. Xu, W. J. de Lange, H. Li, K. Sakai, D. R. Thedens, L. A. Cassis, K. Rahmouni, A. L. Mark, A. K. Johnson, C. D. Sigmund, The brain Renin-angiotensin system controls divergent efferent mechanisms to regulate fluid and energy balance. *Cell Metab.* **12**, 431–442 (2010).

Acknowledgments: We gratefully acknowledge the resources and assistance of the Medical College of Wisconsin Maternal Research Placenta and Cord Blood Bank, Electron Microscopy Core, Mellowes Center for Genomic Sciences and Precision Medicine Center, Genotyping Service Center, Engineering Core, Comprehensive Rodent Metabolic Phenotyping Core, Children's Research Institute Histology Core, Children's Research Institute Imaging Core, and the Vanderbilt University Medical Center Translational Pathology Shared Resource. **Funding:** This work was supported by National Institutes of Health grant HL134850 (J.L.G.), National Institutes of Health grant HL084207 (C.D.S., J.L.G., and A.E.K.), National Institutes of Health grant DK133121 (J.L.G.), National Institutes of Health grant HL150340 (J.J.M.), National Institutes of Health grant HL007852 (M.A.O.), National Institutes of Health grant DK056942 (A.B.F.), American Heart Association Grant 18EIA33890055 (J.L.G.), American Heart Association Fellowship 826132 (M.A.O.), American Heart Association Fellowship 903246 (M.L.R.), American Heart Association Fellowship 898067 (K.B.), Medical College of Wisconsin Clinical and Translational Science Institute UL1TR001436 (J.J.M. and J.L.G.), Children's Research Institute CRI22700 (J.L.G.), American Physiological Society Postdoctoral Fellowship program (K.B.), and Advancing a Healthier Wisconsin endowment (J.L.G. and J.J.M.). **Author contributions:** Conceptualization: M.A.O., J.J.M., and J.L.G. Methodology: M.A.O., K.B., M.L.R., K.-T.L., C.W., K.N.G.-C., A.E.K., C.D.S., J.J.M., and J.L.G. Data collection and analysis: M.A.O., M.C.L., K.B., M.L.R., D.T.B., K.K.W., K.-T.L., K.N.K., C.W., A.B.F., K.N.G.-C., J.J.M., and J.L.G. Funding acquisition: J.J.M., J.L.G., C.D.S., and A.E.K. Supervision: K.N.G.-C., A.E.K., C.D.S., J.J.M., and J.L.G. Writing—original draft: M.A.O. Writing—reviewing and editing: M.A.O., M.C.L., K.B., M.L.R., D.T.B., K.K.W., K.-T.L., K.N.K., A.B.F., K.N.G.-C., A.E.K., C.D.S., J.J.M., and J.L.G. **Competing interests:** J.L.G. is an inventor on patents related to this work filed by the University of Iowa Research Foundation: United States patent no. 9,937,182, filed 10 February 2014, published 10 April 2018; European patent no. 2954324, filed 10 February 2014, published 31 July 2019; European patent no. 2954324B1, filed 10 February 2014, published 31 July 2019. The authors declare that they have no other competing interests. **Data and materials availability:** Placenta RNA sequencing data from *hM3Dq*$^{F/F}$ dam x *Gcm1*-Cre$^{+/-}$ sire pregnancies have been submitted to the GEO repository under accession number GSE221732. All data needed to evaluate the conclusions in the paper are present in the paper and/or the Supplementary Materials.

Submitted 23 January 2023
Accepted 31 October 2023
Published 1 December 2023
10.1126/sciadv.adg8118